Recoil Proton Detection for Radiative Decays of the ϕ Meson

A thesis submitted in partial fulfillment of the requirement
for the degree of Bachelor of Science with Honors in
Physics from the College of William and Mary in Virginia,

by

Lisa J. Kaufman

Accepted for _____
(Honors, High Honors or Highest Honors)

_____
Advisor: Dr. David S. Armstrong

_____

_____

_____

Williamsburg, Virginia
May 2000

Contents

Acknowledgments

I would like to thank the Radphi collaborators that I worked with last summer for all of their guidance as I began my learning process in the world of medium energy physics. I would like to thank Dr. Phil Rubin who sat with me on many long shifts and answered my questions as I tried to figure out what was going on and who always kept us informed about the status of the experiment. I would especially like to thank Craig Steffen who has been an endless resource of information for me about the detectors, the experimental background, and how to write in the logbook. He spent a lot of time on shift with me discussing the trigger logic and simply explaining how things work and has continued the process as I've done analysis and written my thesis. I would like to thank the students from the University of Richmond who welcomed me from the very beginning as we pulled cables through Hall B, especially Laura McGlinchey. I would also like to thank Dr. Jim Kolata who took time out from shifts to talk to me a little bit about graduate school and the CPV.

I would especially like to thank the people closest to me at William and Mary especially during this entire year. I would like to thank my roommate, Jen Wilkes, who was always there for me, day or night, to listen to my stories about my code troubles or there when I made a plot which proved what I had suspected. She has been by my side all this time encouraging me to keep going. I would like to thank Jessica Clark who has become one of my best friends. Having gone through this experience just a few years ago, she was always there to understand what I was going through

and helped me relax when things got rough. My most sincere gratitude goes to my advisor, Dr. David Armstrong, who has helped me tremendously along the way. He was always been there to answer my questions, no matter how stupid I thought that they were. He shared his insight and showed me that I have the ability to do well as long as I set my mind to it. He has helped me understand the experiment from the very start by discussing articles with me and discussing kinematics I felt I should have already known. He has shown unbelievable patience with me, and for that I am grateful. I would also like to extend my deepest thanks to Paul King. Without him, this thesis would never have made it to its final stages. Paul has helped me endlessly by answering my computer questions, LaTeX questions, and general physics questions. He has been a real life saver at times. He always made time for me even though he had no obligation whatsoever to me or my experiment. Thanks again, Paul. I never would have made it without you.

Lastly I would like to thank my parents, my mom and dad, who have patiently listened to me talk about my research even if they didn't know what I was talking about at the time and who raised me to love learning. They have always encouraged me and told me that I can do whatever I want to do. Thank you for believing in me. I would like to thank my sisters, Karen and Debra, who are my best friends. They were only ever a phone call away. They always listened and put things in perspective when I wasn't thinking clearly. They were always there to congratulate me as well, especially when I was accepted into my first graduate school. A sincere thanks goes to my brother, Doug, who helped me find software for my computer so that I wouldn't have to spend late nights in Small or making the trek across campus to Small. I would also like to thank all of my friends here in the physics department. I couldn't have made it this far without them. The late nights of doing problem sets or just the hanging out we did outside of class.

List of Figures

List of Tables

Abstract

An experiment is being done at Thomas Jefferson National Accelerator Facility (TJNAF) to study decays of ϕ mesons produced via the process $\gamma p \rightarrow \phi p$, using the photon beam provided in Hall B. The study of the rare radiative decays of the ϕ meson is dependent on the detection of the ϕ meson as well as its recoil proton. In order to detect these particles, several different detectors are being used. The Barrel Scintillator Detector (BSD) is used to detect the recoil protons of the ϕ production. The timing characteristics and efficiency of the BSD are studied. Evidence of the process $\omega \rightarrow \pi^0\gamma$ is observed and used to determine detector capabilities. The anticorrelation of the proton momentum and ω meson is also observed and confirms detector capabilities.

Chapter 1

Introduction

1.1 The Goal of the Experiment

The radiative decays of the ϕ meson are being studied at Thomas Jefferson National Accelerator Facility (TJNAF) with several goals in mind. These goals include determining the sub-structure of the $f_0(980)$ and $a_0(980)$ mesons, which are poorly understood at present. The observation of the two rare decays, $\phi \to f_0(980)\gamma$ and $\phi \to a_0(980)\gamma$, would be important for meson spectroscopy [1]; but furthermore, the relative rate at which they appear as products of the ϕ decays may help determine whether these states are ordinary $q\bar{q}$ mesons, or rather $qq\bar{q}\bar{q}$ or $K\bar{K}$ molecules [2]. The ϕ mesons are being produced by the process $\gamma p \to \phi p$.

1.2 The E94-016 Collaboration

The experiment, E94-016, at the Thomas Jefferson National Accelerator Facility is a large collaboration of several institutions with a variety of faculty, graduate students, and undergraduate students involved. The institutions contributing to the preparation, implementation, and analysis for this experiment include Catholic University of America, University of Connecticut, Indiana University, University of Massachusetts, University of Notre Dame, Rensselaer Polytechnic Institute, University of

Richmond, University of Virginia, College of William and Mary, and Jefferson Lab.

1.3 Quantum Chromodynamics

Quantum chromodynamics is the theory of interquark forces or the strong interaction [3]. The gluon is the mediating boson which carries the strong force between quarks. There are six different types of strong charge of which three can be carried by the quarks and the other three by the antiquarks. These strong charges are referred to as color and are red, blue, and green along with the corresponding anticolors. Because of the gluon exchange between quarks, free quarks do not appear in nature. Two different configurations of quarks have been observed to date. One configuration is that of three quarks, qqq, called a baryon, e.g. the proton, which consists of two up quarks and a down quark, uud. The second observed configuration of quarks is that of the meson which is made of a quark-antiquark pair, $q\bar{q}$, such as the ϕ meson, which consists of primarily a strange-antistrange pair, $s\bar{s}$. These two configurations, qqq and $q\bar{q}$, are seen consistently and frequently because they are the lowest-energy color singlets (*i.e.* states with no net color).

1.4 Scalar Mesons

Mesons are defined as particles which are made up of a $q\bar{q}$ pair and are categorized into smaller groups based on their quantum numbers. The notation used to describe particles in terms of their quantum numbers is J^{PC} where J is the total angular momentum, P is parity, and C is charge parity. Mesons with $J = 1$ are called vector mesons while mesons with $J = 0$ and positive P are called scalar mesons. If a meson has positive parity, it means that the wave function of a particle is even under spatial inversion of the coordinates. If a meson has negative parity, it changes sign under spatial inversion. A meson with $J = 0$ and negative P is called a pseu-

doscalar meson. The predicted pseudoscalar (0^{-+}), vector (1^{--}), and axial vector (1^{+-}) mesons are easily identified in the experimental spectrum of mesons, while the scalar mesons remain a mystery [4]. The a_0 and f_0 are both 0^{++} particles which makes them appear to fit in the scalar meson category. These particles are being studied as decay products of the ϕ (1^{--}) which is a vector meson. The actual substructures of the a_0 and the f_0 are unknown, but the a_0 and f_0 are generically called mesons because it is known that they are not baryons. This experiment is being done to determine the correct substructure of these particles. The a_0 and f_0 are interesting for several reasons which are discussed in Section 1.5.

QCD predicts several different types of particles with scalar properties (0^{++}). For a given set of quantum numbers J^{PC}, it is expected that there exist nine different combinations, 3×3, of $q\bar{q}$ states if we restrict ourselves to the u, d, and s flavors of quarks. These nine combinations form a nonet. At present, this nonet is well-defined for the vector and pseudoscalar mesons, but the identification of the members of the scalar nonet is problematic and controversial [5]. QCD models predict possibilities of scalar (0^{++}) particles besides $q\bar{q}$. The number of states for the scalar nonet is oversubscribed because there are 11 or 12 possibilities for only nine positions [4]. The lightest glueball, which consists of two gluons bound together by the strong interaction [6], two mesons bound together, e.g. $K\bar{K}$, and the four quark bag, $qq\bar{q}\bar{q}$ are predicted to have scalar quantum numbers. For a detailed review of meson spectroscopy, refer to the paper by Napolitano and Goddfrey [4]. The $a_0(980)$ and $f_0(980)$ are good candidates for the new scalar configurations for several reasons discussed below.

1.5 The a_0 and f_0 Mesons

The a_0 and f_0 mesons are atypical because their masses and widths are too low to be considered as part of the scalar nonet [7]. The width of the meson or any particle

is due to the uncertainty principle and the fact these mesons have a finite lifetime. Better candidates for the scalar nonet are the $a_0(1450)$ and $f_0(1365)$ because of their greater masses and more typical widths. The $\gamma\gamma$ coupling, meaning the possibility for the $a_0(980)$ or the $f_0(980)$ to decay into two photons, is measured to be smaller than expected for a member of the scalar nonet. For this reason, theoretical attention has turned to other explanations of the nature of the $a_0(980)$ and $f_0(980)$ mesons.

As discussed in the previous section, there are several other configurations possible for $J^{PC} = 0^{++}$ state. Since the a_0 and f_0 do not seem to fit very well into the scalar nonet, these other explanations for possible solutions to the question are explored. The possibility of a $K\bar{K}$ molecule has been set forth by Isgur *et al.* [8] as well as the possibility of a four quark bag, $qq\bar{q}\bar{q}$. Close, Isgur, and Kumano [2] have shown that by measuring the branching ratios (the fraction of all decays leading to a particular final state) of the ϕ meson decays, $\phi \to a_0\gamma$ and $\phi \to f_0\gamma$, one can deduce the substructure of the a_0 and f_0. In that paper, the following is predicted about the branching ratios of the $\phi \to a_0\gamma$ and $\phi \to f_0\gamma$:

$$Scalar\ \ q\bar{q}\ \ nonet:$$
$$\frac{\phi \to a_0\gamma}{\phi \to f_0\gamma} = 0 \tag{1.1}$$
$$K\bar{K}\ \ molecule:$$
$$\frac{\phi \to a_0\gamma}{\phi \to f_0\gamma} = 1 \tag{1.2}$$
$$qq\bar{q}\bar{q}:$$
$$\frac{\phi \to a_0\gamma}{\phi \to f_0\gamma} = 9. \tag{1.3}$$

The collaboration at Novosibirsk has obtained initial results on measuring the branching ratio of $\phi(1020) \to \pi^0\pi^0\gamma$ decay, which is dominated by $\phi \to f_0\gamma$. This experiment compares the absolute branching ratio of the ϕ to the branching ratio of the $f_0(980)\gamma$. In that study, the measured branching ratio of $\phi \to f_0\gamma$ was found to

be five times larger than the $q\bar{q}$ and $K\bar{K}$ model predictions. They concluded that the f_0 is significantly made up of $qq\bar{q}\bar{q}$ while not excluding contributions of other quark configurations to the nature of the f_0 [9].

Until the Novosibirsk results became available, these decays were unobserved, only upper limits on the branching ratios were known. These upper limits, along with the main decays modes of the a_0 and f_0 particles, are summarized in Table 1.1, Table 1.2, and Table 1.3 [10]. In this experiment, the final photonic states of the decays are observed, e.g. $\phi \to f_0\gamma$, $f_0 \to \pi^0\pi^0$, $\pi^0 \to \gamma\gamma$ generating a five photon final state.

Decay Modes $\phi \to$	Branching Ratio
K^+K^-	$(49.1 \pm 0.8)\%$
$K_L^0K_S^0$	$(34.1 \pm 0.6)\%$
$\rho\pi + \pi^+\pi^-\pi^0$	$(15.5 \pm 0.7)\%$
$\omega\gamma$	$< 5\%$
$f_0(980)\gamma$	$< 1 \times 10^{-4}$
$a_0(980)\gamma$	$< 5 \times 10^{-3}$

Table 1.1: Main decays of the ϕ meson [10].

Decay Modes $a_0 \to$	Branching Ratio
$\eta\pi$	dominant
$K\bar{K}$	seen
$\gamma\gamma$	seen

Table 1.2: Decays of the a_0 meson [10].

Decay Modes $f_0 \rightarrow$	Branching Ratio
$\pi\,\pi$	dominant
$K\,K$	seen
$\gamma\gamma$	$(1.19 \pm 0.33) \times 10^{-5}$
e^+e^-	$< 3 \times 10^{-7}$

Table 1.3: Decays of the f_0 meson [10].

Chapter 2

Experiment E94-016

2.1 Overview of the Experiment

In order to study the rare radiative decays of the ϕ meson, it is necessary to produce the ϕ with a well understood process. In this experiment, a 5.5 GeV electron beam is used to produce up to a 5.5 GeV photon beam in Hall B of the Thomas Jefferson National Accelerator Facility which then interacts with a Be target and can produce the ϕ meson ($\approx 70\phi/s$) by way of the photoproduction process $\gamma p \rightarrow \phi p$. The proton and decay products of the ϕ are then detected by the several detectors of the experiment which will be discussed in detail below.

Two major processes that should be considered when describing what happens when a γ-ray hits a nucleus are the photonuclear effect and pair production. In the photonuclear effect a photon interacts with a field of a nucleus to produce an excited nucleus in the atom,

$$\gamma + A \rightarrow A^*.$$

Another process that can occur under these circumstances is that a photon pair-produces to form a bound state of quarks (specifically, a $q\bar{q}$ pair). As discussed earlier, this bound state is known as a meson. In this experiment, we are looking for the ϕ meson which is made up predominantly of an $s\bar{s}$ pair. The photoproduction process

mentioned above is a good candidate for this production because the photon and the ϕ have the same quantum numbers, $J^{PC} = 1^{--}$ and zero charge. Photoproduction is an appropriate process for the production of ϕ mesons because it is dominated by vector mesons. Producing ϕs using this process is beneficial because the reaction rate is high and the ϕs are boosted so that it is easier to detect each of the decay photons. The process of e^+e^- collision used at Novosibirsk has its advantages and disadvantages. For instance, in the process of colliding a positron and an electron one can pick the exact energy of the particles to match the ϕ's rest mass. This allows a very clean production of the ϕ without producing other background particles. On the other hand, the reaction rate is very small. Also since the ϕs are produced at rest in the lab, it is difficult to detect a low energy photon to which the ϕ decays, e.g. as part of $\phi \to a_0\gamma$ where this photon would only be approximately 40 MeV.

2.2 The Accelerator at TJNAF

Thomas Jefferson National Accelerator Facility (TJNAF) in Newport News, VA is a lab supported by the Department of Energy. The central research mission of the lab is to probe the nucleus of the atom in order to learn more about the quark structure of matter. The accelerator produces an electron beam which is used to probe the structure of the target or to produce other particles whose interactions and decays can be studied. The accelerator at TJNAF is unique because the lab uses superconducting radio-frequency accelerating cavities to produce a continuous-wave electron beam[1].

The accelerator is a 7/8-mile racetrack in which the electron beam can travel up to five times around, gaining energy with each pass. The beam can be separated into the

[1]The beam is not actually continuous, but because the pulses occur at a frequency of 2 GHz, the beam is essentially continuous.

three different experimental halls: A, B, and C; each hall can have a different beam energy depending on which pass of the beam is selected. This enables the halls to run simultaneously at three different energies specific to the needs of the experiments in each hall. The present data were taken using a 5.5 GeV electron beam and a beam current of between 125 nA and 130 nA.

2.3 Hall B

Experiment 94-016 at TJNAF is located in Hall B, downstream of the CLAS (CEBAF[2] Large Acceptance Spectrometer) in the hall alcove. One feature that distinguishes Hall B from the other two halls at TJNAF is that it can use the electron beam to produce a high-energy tagged photon beam. The E94-016 collaboration uses this technology in order to photoproduce the ϕ meson. The electron beam provided by TJNAF produces a tagged photon beam of up to 5.5 GeV energy, and of intensity $5 \times 10^7 \gamma/s$ for the 25% most energetic tagged photons [11] by way of the bremsstrahlung process. In order to get a photon beam from an electron beam, the electron beam traverses a material acting as a radiator, in this case tungsten with a thickness between 2×10^{-4} and 3×10^{-4} of a radiation length ($X_0 = 0.35$ cm), in which the electrons are negatively accelerated and emit photons that appear due to the change in energy. This radiation process is called bremsstrahlung radiation, which means "braking radiation." Electrons are deflected from the primary beam direction by a dipole magnet located after the radiator while the radiated photons continue in the original beam direction. These photons are "tagged" in Hall B by the photon tagger. The electrons are the particles actually detected, but conservation of energy and knowledge of the electron beam allows a determination of the photon

[2]CEBAF stands for Continuous Electron Beam Accelerator Facility and was the previous name for TJNAF.

energy via the measurement of the electron's final energy. The photon tagger will be discussed in more detail in Section 3.3.1.

2.4 History of E94-016

This experiment has had four engineering runs beginning in May 1997. These engineering runs were intended to determine the detectors' capabilities and efficiencies, the capabilities of the electronics, and the ability of the experiment to provide the proposed results. During the summer of 1999, a new detector setup was tested. A barrel scintillator detector (BSD) replaced the previous recoil proton detector because of its increased detection solid angle and resolution of the proton position. The barrel gamma veto (BGV) was also installed in order to detect photons that may not reach the lead glass detector (LGD). By the end of the summer, both of the new detectors were commissioned and are being used in the scheduled data taking run which begins May 2000. During this run, the experiment will have three months of data taking with a high intensity photon beam.

Chapter 3

Experimental Apparatus

3.1 Interactions and Processes of Particle Detection

The section provides a brief overview of the physics involved with photon and charged particle detection in the energy regions of interest for this experiment.

3.1.1 Interactions of Photons in Matter

When a γ-ray (>1 MeV) interacts with a material, three different processes can take place. The first process called photoelectric absorption where a photon and an atomic electron interact, and the electron absorbs the energy of the photon and is thereby ejected from the atom,

$$\gamma + e^- \rightarrow e^-. \tag{3.1}$$

Photoelectric absorption varies as $1/{E_\gamma}^3$, where E_γ is the photon energy, and rarely occurs at energies of relevance here (150 MeV-6 GeV) because the energy of the photon needs to be close to the binding energies of the electron.

The second process is Compton scattering, the probability of which varies as $1/E_\gamma$. Compton scattering is the process where a photon elastically scatters from an atomic

electron,

$$\gamma + e^- \rightarrow \gamma + e^-. \tag{3.2}$$

The third process that can occur is pair production. The process of pair production at these high energies dominates because it is essentially independent of energy. In this process a high energy photon is converted into an electron-positron pair in the field of a nucleus (A) which is necessary to conserve energy and momentum:

$$\gamma + A \rightarrow e^+ + e^- + A. \tag{3.3}$$

The photons can cause electromagnetic showers in a material because they can produce electron-positron pairs which can then undergo bremsstrahlung (discussed below), creating more photons which can again pair-produce until there is not enough energy left to radiate.

3.1.2 Interactions of Charged Particles in Matter

Charged particles traversing a material can lose energy mainly in three different ways, namely, ionization, Cerenkov radiation, and bremsstrahlung.

Ionization is the process of removing an electron from an atom. A charged particle traveling through a scintillating material will transfer some of its energy to the atoms in the material causing them to ionize, consequently, losing energy as it traverses the material. The light emitted from ionization is usually in the blue visible and UV (ultra-violet) region and can be detected by photomultiplier tubes.

Cerenkov radiation occurs when a charged particle moving through a material is moving faster than the speed of light in that medium. The emitted light (blue and UV) can also be detected using photomultiplier tubes.

Bremsstrahlung is the process by which a charged particle passes near a nucleus of some material and radiative energy loss occurs thereby emitting photons. This process creates electromagnetic showers as previously discussed in Section 3.1.1.

The scintillator detectors use the process of ionization to gather information about the particle passing through it while the lead glass calorimeter detects Cerenkov radiation as the particle produces an electromagnetic shower.

3.2 Overview of the Detectors

This experiment requires the production of the ϕ meson, but $\gamma p \rightarrow \phi p$ is not the only reaction that occurs when a photon hits the Be target. The ϕ can decay in many different ways (see Table 1.1), therefore, a detector needs to be able to select signal from background, have a large acceptance for the reaction of interest, and needs to be able to detect many photons. For these reasons, experimental setups are often quite complicated. In this experiment there are six different detectors being used. The first detector is the photon tagger used to detect the electrons that radiate and consequently identify the photon that was radiated. Next along the beamline is the upstream particle veto (UPV) which is used to detect charged particles coming from upstream before the beam has interacted with the target. The next detecter is the barrel scintillator detector (BSD) which surrounds the target and is used to detect the recoil proton. The barrel gamma veto (BGV) is a calorimeter surrounding the BSD which detects wide-angle photons. The charged particle veto (CPV) is located in front of the lead glass detector (LGD) in order to detect charged particles that may have been produced from the target. The lead glass detector is a large calorimeter used to detect the photons that are decay products of the ϕ, and which create electromagnetic showers in the lead glass. Each of the detectors is discussed in more detail below; the setup is depicted schematically in Figure 3.1.

Several different types of detectors and other measurement tools are used in this experiment including photomultiplier tubes, scintillators, and electromagnetic shower detectors.

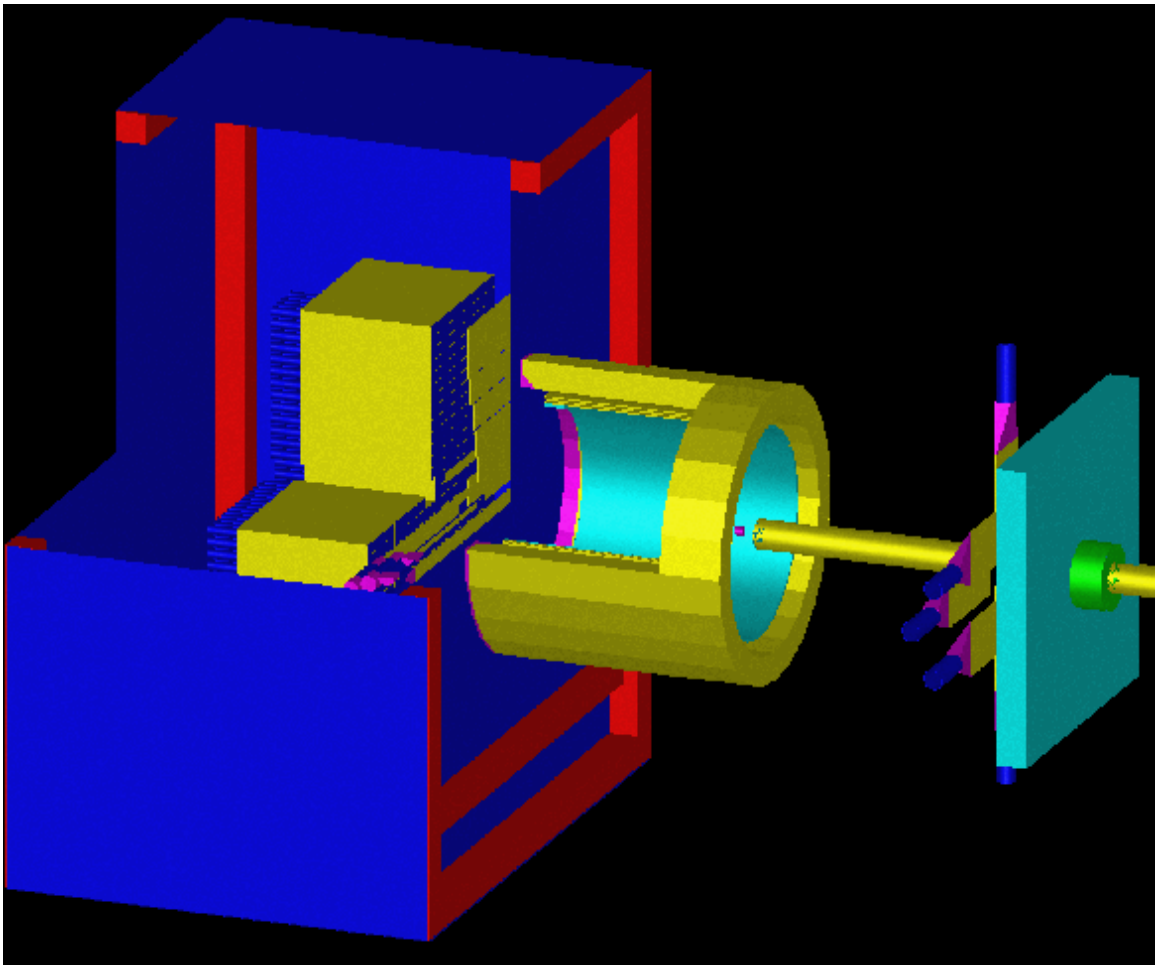

Figure 3.1: Schematic of the experimental setup. From right to left we see the lead shielding wall, the UPV, the beam pipe, the target, and then the barrel, which is cutaway to see the BSD inside the BGV. Following the barrel is a light tight casing, cutaway to see inside, housing the CPV and LGD also cutaway to see inside.

Photomultiplier tubes are located at the end of scintillators and other counters in order to detect the ionized or radiated light from the counter. The visible light from the counter frees electrons by the photoelectric effect from a photocathode layer at the internal surface of an evacuated glass or quartz tube. The photoelectrons are accelerated from the cathode onto the first dynode (in a chain of dynodes) which is a material with a high probability of secondary electron emission. This process

continues through the chain of dynodes, and the output is read out as a voltage signal by analog to digital converters.

Plastic scintillators are used in several detectors in this experiment including the photon tagger, the UPV, the CPV, and the BSD. Scintillators are used to convert ionization energy into visible light and to transport the light to the photomultiplier tube. Scintillators must be polished to be completely smooth so that there is total internal reflection in the material to prevent losing any of the light produced from ionization. Plastic scintillators are usually made into rectangular strips and are made to provide a uniform light yield over the entire length. In this way, the photomultiplier tubes should detect the same amount of light irrespective of the location through which the particle passed. Plastic light guides are used to transport the light from the scintillators to the photomultiplier tubes with approximately total internal reflection so that no light is lost.

The electromagnetic shower detectors in this experiment are the barrel gamma veto and the lead glass detector. The photons that move through these detectors pair produce while the charged particles undergo bremsstrahlung. This creates the electromagnetic "shower" in these detectors. This process will continue as long as the probability of a photon to undergo bremsstrahlung is above the critical energy of the detector. If the detector elements are made to be several radiation lengths long as to contain the entire electromagnetic shower, it will measure the total energy of the particles which entered. The Cerenkov light produced from the charged particles moving with velocity, $v = \beta c$, which is greater than c/n, where n is the index of refraction of the detector material, is then detected by photomultiplier tubes placed at the end of each of the counter segments.

3.3 Experimental Setup

3.3.1 The Photon Tagger

A detailed discussion of the design and performance of the photon tagger can be found in [11]; a brief outline is presented here. Electrons that undergo bremsstrahlung in the material deflect in the magnetic field in proportion to the energy of the produced photons. The electron is tagged by the photon tagger which is divided into several segments of plastic scintillators corresponding to fractions of the original beam energy. In the present case, the first nineteen segments correspond to the 25% most energetic photons with energies between 4.25 and 5.5 GeV. The unaccelerated electrons go into a beam dump. The tagger is the first real detector in this experiment because it detects the production of a photon; therefore, it sets the timing for the rest of the event.

Each of the photon tagger scintillators are constructed as one rectangular piece of plastic with a photomultiplier tube on each end. For simplicity, the trigger only receives information from the left side which is sufficient because both photomultiplier tubes should detect light when an electron goes through the scintillator. The tagger performs at a rate of up to $5 \times 10^7\ \gamma/s$.

3.3.2 The Upstream Particle Veto (UPV)

The UPV is a detector consisting of eight plastic scintillator segments and is located in front of the Be target of the experiment. The UPV detects charged particles coming from upstream produced, for example, by beam photons interacting with the beam vacuum pipe or residual gas in the beamline. An event is vetoed by the trigger electronics hardware if one or more of these segments fires, because it means that beam interactions from upstream could contaminate the event. The UPV is segmented in order to control the rates that the photomultiplier tubes fire for each scintillator. If

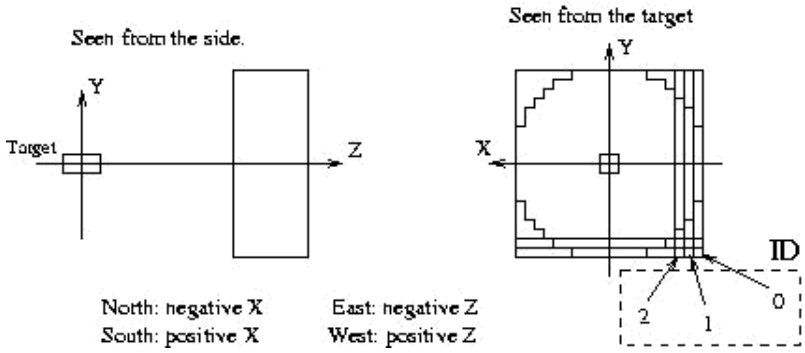

Figure 3.2: Coordinate system for E94-016.

the UPV were not segmented, the photomultiplier tube would detect so much light that it would begin to saturate. By segmenting the UPV, each photomultiplier tube can run more efficiently. The UPV is also segmented in order to accurately measure the timing of charged particles passing through the detector. Because it takes time for light to travel through the scintillators to the photomultiplier tubes, it is necessary to have small pieces of plastic scintillator to reduce the effect this would have on the time of an event. The UPV is discussed in more detail in [12].

3.3.3 The Barrel Scintillator Detector (BSD)

The barrel scintillator detector is crucial for this experiment because it enables us to detect the recoil protons from the process $\gamma p \to \phi p$. Previously, this detector was used as part of the Jetset experiment at CERN (European Organization for Nuclear Research) in order to detect charged particles. The BSD efficiently detects protons because of its large solid angle. It locates where the protons hit with respect to the z-axis, along the beam direction, and the azimuthal angle, ϕ (not to be confused with the meson; this distinction should be apparent from the context), because of its geometry (see Figure 3.2 for a definition of the coordinate system). The BSD consists of three different layers of plastic scintillators. There are 24 straight counters each of

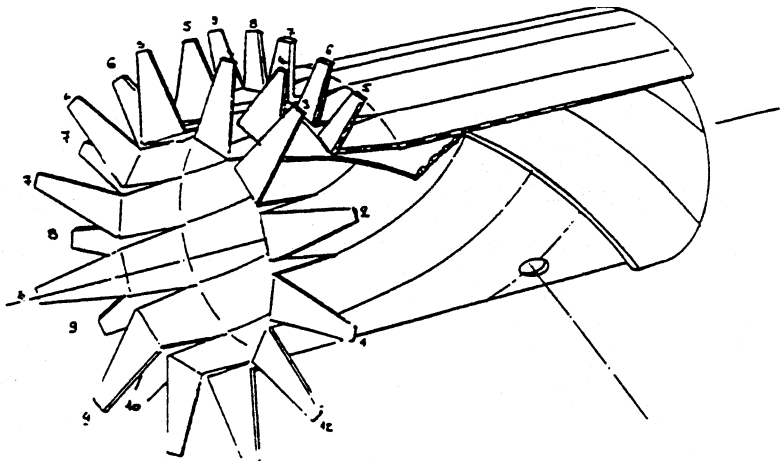

Figure 3.3: The three layers of the BSD.

70 cm [13] oriented along the beam direction which cover the entire circumference of a circle surrounding the Be target. There are 12 counters that go helically to the right and 12 counters that go helically to the left covering the entire cylinder as well. The innermost layer of scintillators is the helically left set of counters, then the helically right, and on the outermost layer of the BSD are the straight counters, see Figure 3.3. Each layer of scintillators is 5 mm thick [13]. The location where a counter from each of the three layers overlap is called a pixel and enables a determination of the location of a proton in z and the angle ϕ.

The BSD surrounds the Be target so that when a photon interacts with a proton within the target, the proton can be detected at any angle ϕ and for a large range of θ, $-135° \leq \theta \leq -45°$ and $45° \leq \theta \leq 135°$. When there is an event, one counter in each layer should fire in order to define a pixel and locate the proton. The photomultiplier tubes located at the upstream ends of the scintillation counters will detect the amount of light produced in each counter; therefore, protons can be detected by the amount of energy from ionization that is deposited in the counters. Because the protons are moving more quickly than minimum ionizing particles such as energetic electrons, the threshold can be set higher on the counters so that the higher energy-loss of the

protons and fewer minimum ionizing particles can be observed.

3.3.4 The Barrel Gamma Veto (BGV)

The BGV is a calorimeter segmented into 24 azimuthal segments made of 50% lead alloy, 35% scintillating fibre, and 15% epoxy [14] that surrounds the BSD. The BGV is used to detect photons that emerge at a very wide angle and would therefore not make it into the lead glass detector. In this detector an electromagnetic shower is produced by the photons that are a result of the ϕ decay. Photomultiplier tubes absorb the Cerenkov light produced by the shower and are located at both the upstream and downstream ends of the BGV segments. The BGV can be used as a veto or a detector in this experiment. As a veto, if there is more than one hit in the BGV (allowing one hit for the proton going through), an event is vetoed in the software because not all of the photons of an event are contained in the LGD. The BGV can also be used as a detector to include the photons from the BGV with the photons in the LGD in the analysis. For more information about the BGV see [15].

3.3.5 The Charged Particle Veto (CPV)

The CPV is a detector consisting of 30 different plastic scintillators used in order to find any charged particles that could possibly continue through to the LGD. Therefore, it is placed in front of the LGD. Since the experiment is only looking for neutral particles (*i.e.* photons from the decay of the ϕ meson), an event can be vetoed or regarded as invalid if there is a charged particle in the detector. This rejection (unlike that for the UPV) is done only in the software, not by the trigger electronics in hardware. It is necessary for the CPV to be a segmented detector in order to control the rates on the photomultiplier tubes and to accurately measure the timing of the charged particles passing through the detector. The CPV can be mapped onto

the LGD in order to identify where charged particles may have deposited energy in the LGD. The segments help provide a more precise location of these particles so that charged particles are not mistaken for photons in the LGD.

3.3.6 The Lead Glass Detector (LGD)

The LGD is a calorimeter that is 1m $\times$ 1m $\times$ 41 cm consisting of 620 lead glass blocks in which the photons from the ϕ decay produce electromagnetic showers. There is actually an array of 28 rows $\times$ 28 columns of blocks in the LGD, but only 620 are connected to photomultiplier tubes. The lead glass blocks are made of 45% PbO and 43% SiO_2 with an index of refraction of 1.62 [16].

As the electron-positron pairs, from $\gamma \rightarrow e^+e^-$, move through the lead glass, they produce Cerenkov light because these particles are traveling faster than the speed of light in this material ($v > 1.85 \times 10^8 \frac{m}{s}$). The electrons will undergo bremsstrahlung in the lead glass until they reach the critical energy of 12 MeV where ionization loss becomes important, and the showering process ends [16]. The photomultiplier tubes at the end of each lead glass block absorb this light and convert it into a voltage signal that the electronics then records and in return can be converted into an energy value in software. The invariant mass of a particle in the lead glass can be reconstructed from the energy and momenta of the photon clusters in the LGD. A cluster is defined as a contiguous group of blocks whose energy is above a certain threshold.

The algorithm by which the software identifies a cluster is known as the "clusterizer." A detailed discussion of the clusterizer is found in [16]; only a brief outline is given here. The clusterizer is a pattern searching algorithm consisting of three levels that looks for local maxima in the energy deposition in the LGD. The level one search looks for a center block with high energy deposition along with its bordering neighbors forming a 3 block $\times$ 3 block cluster. This search continues until there are no blocks

left with energy greater than 350 MeV which are not already part of a cluster. The second level search looks for blocks within 10 cm of only one cluster but not yet part of another cluster, called associated blocks. The second level also looks for shared blocks that are defined to be within 10 cm of two or more clusters but not yet part of one. The third level search essentially repeats the level one process replacing the 350 MeV threshold with the requirement of 150 MeV of energy deposited in a block to define a cluster. The Event Display, discussed in more detail below, pictorially shows the clusters (see Figure 5.5). These clusters are then converted into photons as discussed in [16]. The photon momentum is determined by

$$\vec{p} = \frac{\vec{r}}{|\vec{r}|} E_c, \tag{3.4}$$

where $\vec{r}$ is the measured position of the cluster and E_c is the cluster energy. The position of the cluster is not the impact coordinate of the photon on the face of the lead glass; therefore, a depth correction must be made to the photon momentum. The position of the cluster is not the impact coordinate of the photon because it take some time for the photon to travel within the lead glass before it first pair produces, inducing an electromagnetic shower. The actual radial position of the photon, $\vec{r}_{act}$, at the face of the glass is therefore given by

$$\vec{r}_{act} = \vec{r}_c - D \sin\theta \frac{\vec{r}_c}{|\vec{r}_c|} \tag{3.5}$$

where $\vec{r}_c$ is the position of the cluster and D is the depth of the shower maximum (see Figure 3.4). An iterative technique used to determine $\vec{r}_{act}$ is discussed in detail in [16].

Once $\vec{r}_{act}$ has been decided, the calibration constants of the individual lead glass blocks are determined by converting the ADC (analog to digital converter) value to an energy in units of GeV. Consequently, the energy of each photon can be determined.

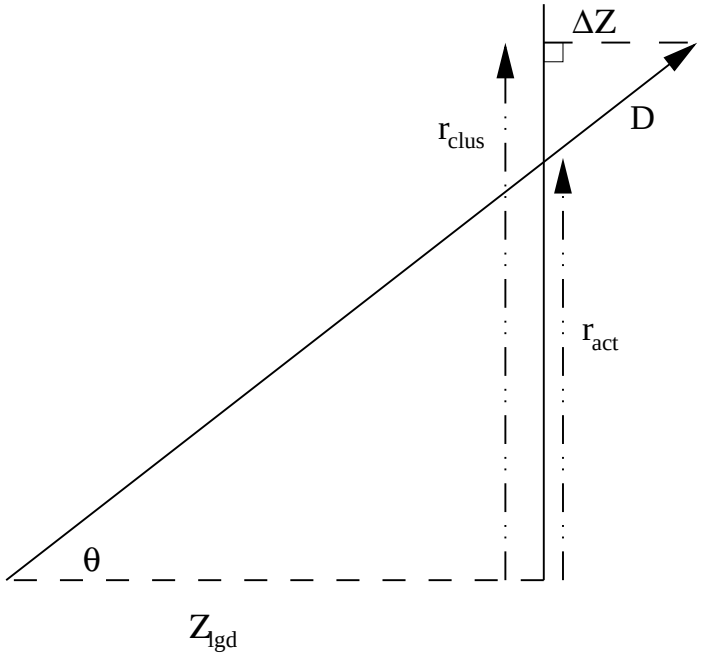

Figure 3.4: The geometry of the cluster depth correction.

3.4 Detector Acceptance

The expected acceptance of the different decay modes for this experiment as determined by Monte Carlo simulation is shown in Table 3.1 [1]. These acceptances are based on being able to find the right number of photon clusters in the LGD. These acceptances also depend on the solid angle of detection. In order to observe all of these modes, all of the photons of the decays must be detected in the lead glass. Because the experiment only detects all-neutral branching ratios, acceptances are higher or lower according to the dominant decays for a particular meson.

Decay Mode	Acceptance (%)
$\phi \to \eta\gamma$	8
$\phi \to \pi^0\gamma$	11
$\phi \to a_0\gamma$	3
$\phi \to f_0\gamma$	5
$\phi \to \eta'\gamma$	14
$\phi \to \omega\pi^0$	2
$\omega \to \pi^0\gamma$	17
$\omega \to \eta\gamma$	23
$\rho \to \pi^0\gamma$	32
$\rho \to \eta\gamma$	28

Table 3.1: Acceptance of neutral decay modes of light vector mesons [1].

Chapter 4

Electronics

4.1 Analog to Digital Converters

The analog to digital converters (ADCs) of the BSD digitize the amplitude of the signals read from the photomultiplier tubes representing the amount of ionization that occurred in the individual scintillators of the BSD. When there is a peak in the ADC spectra representing the ionization of the proton, as seen in Figure 4.1 at channel 250, it can be concluded that a proton went through the detector. Having a proton go through a pixel of the BSD is a necessary but not sufficient condition for knowing that a ϕ was produced. Evidence of the proton in the BSD is a reason to look at the lead glass detector in search of the multi-photon events that represent the ϕ decays of interest.

The ADC is also used for monitoring the performance of the BSD channels. It is expected that a proton passing through the BSD will ionize evenly in each layer of the detector; therefore, the ADC value in each layer of the detector should be similar. Also, the peaks in the ADC spectra should be in the same place as long as the photomultiplier tubes are working properly and have been properly gain-balanced. If the peaks begin to move, then there is a possibility that the photomultiplier tubes are saturated and need to be replaced or have their voltages reset.

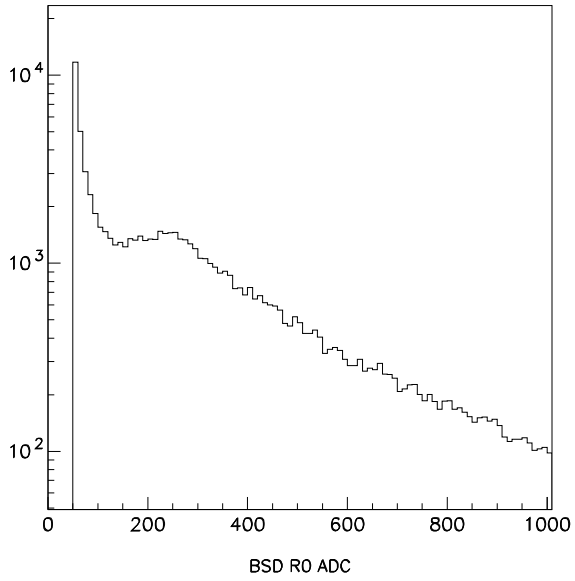

Figure 4.1: The ADC spectrum (events vs. ADC bin number) for a typical counter of the BSD.

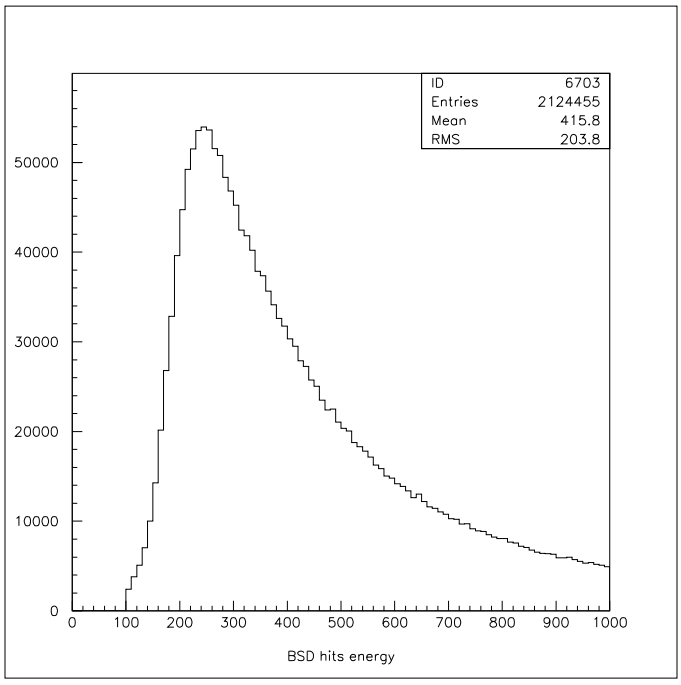

Figure 4.2: ADC spectrum of high-rate run with threshold at channel 100.

The pedestal of the particular photomultiplier tube sits at channel 50 in Figure 4.1. The reason why the pedestal is above zero is because of the use of unsigned integers in the ADC electronics; therefore, any jitter in the tubes when the pedestal is set above zero reads the correct values. A good hit in the BSD requires a hit in time with the tagger, and the ADC signal is required to be above the discriminator threshold. The discriminator threshold sets a minimum value related to energy deposited in the counter in order for the ADC to be considered a good hit. A minimum ionizing peak is visible at channel 250, but the protons typically ionize more; therefore, the threshold is set at about the middle of this peak. The threshold is placed at channel 100 so that the ionization peak can be easily identified at channel 250 in Figure 4.2

4.2 Time to Digital Converters

One of the most important conditions for considering an event to be valid is whether the BSD and the tagger have hits that occurred in coincidence, *i.e.* the tagged photon and recoil proton were in time coincidence. A discriminator is a component of the electronics triggered by the leading edge of an analog pulse. Once this pulse is larger than a specified threshold, the discriminator sends a logic signal to the TDC, specifying a hit. The TDCs that are being used for the BSD are common stop TDCs, which means that there is a clock, in this case a 2 GHz clock, that goes through the channels and marks everywhere that it sees a hit until it gets a signal from the trigger and stops. The trigger time is usually defined by tagger time because the tagger signal is designed to reach level 1 of the trigger logic last of all of the trigger's components. Once the TDC receives the stop signal, it then outputs the bin number of each hit corresponding to the time difference between the stop and that hit up to a specified maximum number of hits. A typical time spectrum is shown in Figure 4.3. The peak in the TDC spectra corresponds to the coincidence of the tagger and

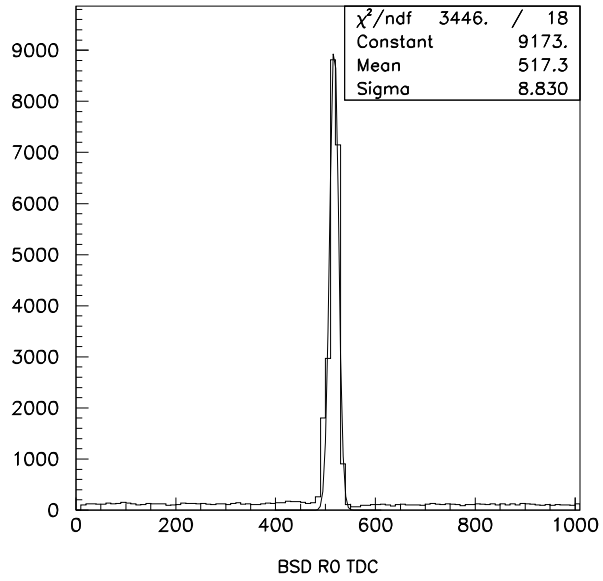

Figure 4.3: Time spectrum of typical BSD counter, relative to the trigger time, in TDC channels (1 channel = 0.5 ns). A Gaussian fit is superimposed.

the BSD. The σ of the fit in Figure 4.3 is channel 8.8 which means that the timing resolution is only good to 4.4 ns (each channel equals 0.5 ns). In order to improve the TDC resolution, further study of the tagger and the trigger is required.

4.3 The Trigger

The trigger has three different requirement levels in the hardware, with each level becoming more selective on the data. The first level of the trigger requires there be at least one hit in each of the layers of the BSD (Figure 4.4), a hit in the tagger, and no hit in the UPV. The second level of the trigger requires that there be a pixel in the BSD and at least one block with energy above a certain threshold in the LGD. The third level of the trigger requires that the approximate total energy in the LGD is a minimum of roughly 2 GeV.

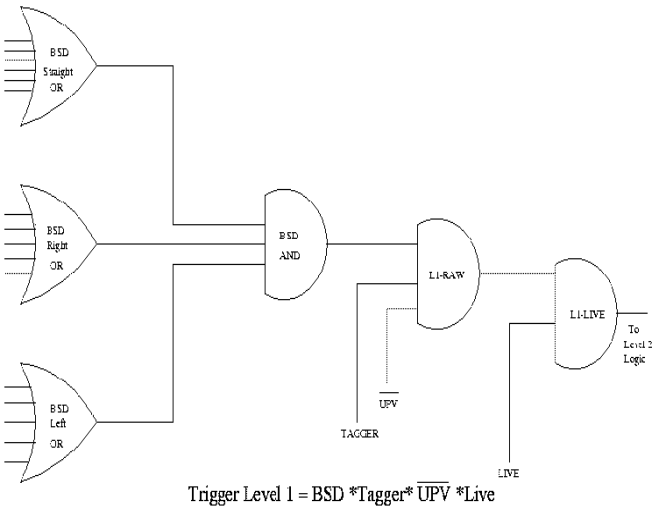

Figure 4.4: Logic for the level one trigger requiring a triple coincidence in the BSD and a hit in the tagger at the same time.

Because each level of the trigger becomes more selective, the actual rates of each level decrease as fewer data meet the requirements. These rates are summarized in Table 4.1. Level 1 RAW is defined as the rate at which the TAG*BSD was firing (see Figure 4.4). The Level 1 LIVE rate is when the above coincidence was true and the data acquisition was live. The Level 2 PASS is the number of events that satisfy the level 2 requirements described above. The Level 3 PASS is the rate at which the data were written to disk. The deadtime (the amount of time the data acquisition is unavailable to write anything to tape) is a result of how long it takes to write the data to disk as well as the time it takes for logic gates to be sent and travel through all of the electronics. The deadtime is calculated as $1 - \frac{\text{Level 1 LIVE rate}}{\text{Level 1 RAW rate}}$. With new improvements being made in Hall B, putting in faster cables, new TDCs, and shortening the ADC gates, it is expected that the deadtime will decrease to 35-40%

Trigger Level	Rate
Level 1: RAW	575 kHz
Level 1: LIVE	250 kHZ
Level 2: PASS	5200 Hz
Level 3: PASS	70 Hz
Deadtime	57%

Table 4.1: Trigger rates and deadtime at $5 \times 10^7 \gamma/s$ in the tagger, nominal beam rate.

at full beam rate of 125-130 nA and $5 \times 10^7 \gamma/s$ in the tagger.

The trigger logic is set up such that the tagger signal is the last signal that the Level 1 RAW AND gate receives; therefore, the trigger time is defined by the tagger. Unfortunately for some events or combinations of BSD channel plus tagger channel, the BSD signal comes in later than the tagger, setting the trigger time for that event. This situation will be discussed in more detail in Chapter 6.

Chapter 5

Software

5.1 RODD

RODD is the off-line data analysis software for TJNAF E94-016 and stands for Radphi Off-line Data Decoder. For a detailed description of the RODD program, see [17]. The two main purposes of RODD are to unpack the data and to serve as a first level of analysis. RODD reads raw data from the data acquisition tapes consisting of "itape" files.

RODD will read each data file and write out the decoded information to a new itape file, thereby "unpacking" the data. The raw data is grouped logically into events which contain encoded output from the various detector components. RODD is written to interpret these data (words on tape) from each hardware module (e.g. ADCs and TDCs) and decode the data into meaningful information to the user. At this point, the raw hardware output is mapped to the specific detector component to which it belongs. Each word on the tape is associated with a particular module number in the hardware as well as a channel number of the ADC or TDC module, which is then translated into a channel of a particular detector (e.g. TDC module 3, channel 15 may correspond to Tagger, left 15.). RODD then creates a group (a structure in C) to store the detectors' TDC information and a separate group for

their ADC information. Once the user has these groups, more useful data analysis can be done.

Not only does RODD create these groups, but it also provides a first look at the data. RODD uses HBOOK (which is part of the CERN library) to create histograms of the ADC (see Appendix B) and TDC information for each channel of each detector. These histograms are an indication that each of the detectors is working properly. It is important to make sure that each element of each detector has a proper ADC or TDC readout. If the ADC or TDC peaks are not similar within a certain detector, it can instantly be seen that there is a problem with a channel of the detector by looking at these histograms. The Event Display is also another form of this first step of analysis. More in-depth analysis can be conducted by modifying individual versions of RODD with cuts on the data and creation of new histograms.

5.2 Event Display

The Event Display, as previously mentioned, provides a graphical representation for each event of the data. The compiled program consists of five files written in C, where one contains the main program and the other four are minor routines that control the surroundings of that main program. The graphics in the event display is based on Hv, HotViews; Hv is a library package of extra, mainly graphics C routines, developed by D. Heddle [18]. Hv is layered on top of X and OSF Motif. The picture provided by the event display includes ADC and TDC information.

The photon tagger is the first of the displays, and shows only TDC information because we know the energy of the photon based on which segment of the tagger the electron hit. The tagger display shows the time for the left and right photomultiplier tubes by the color of the segment. When the left and right colors match, it means that a valid hit was made in the tagger (see Figure 5.1).

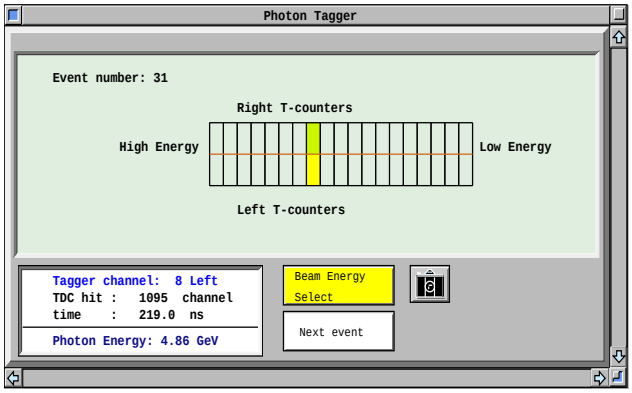

Figure 5.1: The tagger view. The color corresponds to the timing of a hit.

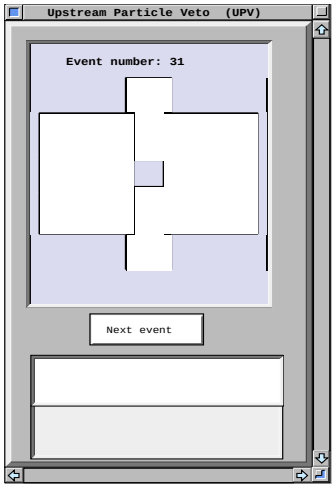

Figure 5.2: The UPV view with no hit because the UPV is a veto in the hardware.

The UPV view (Figure 5.2) shows both ADC and TDC information in order to tell where a charged particle went through the detector as well as the time in order to determine whether it may have actually contaminated an event. The color corresponds to the amount of ionization in the UPV while the vertical lines correspond to a hit in time with the tagger. Because the UPV is used as a veto at the level of the trigger, a hit is rarely seen in the UPV when looking at the event display.

The BSD view (Figure 5.3) is a picture of the BSD cylinder unfolded from S0 ($\phi =$

$15° - 30°$) to S23 ($\phi = 0° - 15°$). The BSD view displays the overlap of the right (R), left (L), and straight (S) scintillators. The different overlap regions of the R, L, and S scintillators correspond to individual pixels. The color in each layer corresponds to the ionization of the proton in each layer. For this reason, a pixel corresponding to a proton track should have similar coloration in each of its layers. The horizontal hatching corresponds to hits in time with the tagger. The display gives the R, L, and S combination for a pixel as well as the timing and ADC value for each counter. A good hit in the BSD should have similar coloration in each layer as well as similar timing in coincidence with the tagger.

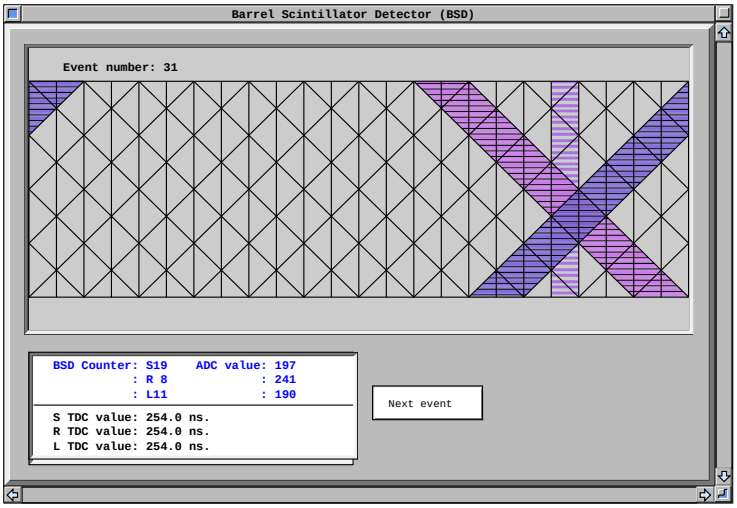

Figure 5.3: The BSD unfolded view. The overlay of 3 scintillator counters shows a pixel. The color corresponds to the ADC value and the hatching to an in time hit.

The CPV view (Figure 5.4) shows the 30 segments of the CPV with ADC and TDC values. The CPV view is similar to the BSD and UPV in that the color of each segment corresponds to the amount of ionization of a charged particle passing through. The TDC values in time with the tagger are signified by the vertical lines. The CPV view and the LGD view correspond to their actual sizes in order to project charged particles from the CPV onto the same area of the LGD. If a CPV hit is seen

in the same place as a hit in the LGD, then the event may be chosen to be vetoed.

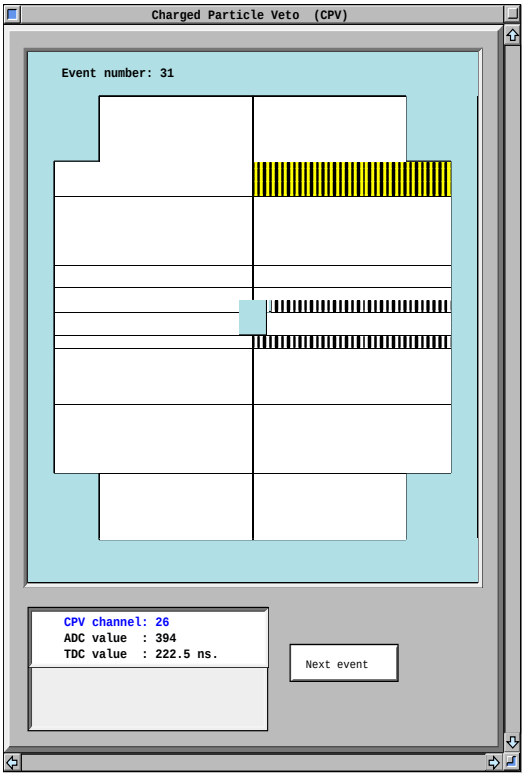

Figure 5.4: The CPV view. The colored blocks represent ADC hits and the hatching represents an in time hit.

The BGV and LGD are on the main view of the event display (Figure 5.5). The BGV is a 24 sided regular polygon that surrounds the LGD and BSD on the main view. The BGV has photomultiplier tube readouts on both the upstream (inner ring) and downstream (outer ring) ends of the detector in order to deduce the location of the photon. The segments' color corresponds to the energy of the photon passing through it. If there is a white dash in the middle of the segment, the photon hit is in time with the tagger.

The LGD view shows the amount of energy deposited in the lead glass blocks with lower energy hits close to white and higher energy closer to red on the color

scale. The event display also has its own version of the clusterizer which draws circles around the photon clusters. The LGD view also displays the invariant masses of user-selectable combinations of the photon clusters along with their x and y coordinates. This information is useful to determine the masses of the reconstructed particles such as the π^0, ϕ, and ω as well as for seeing the correlation of the momentum between the photons and the proton.

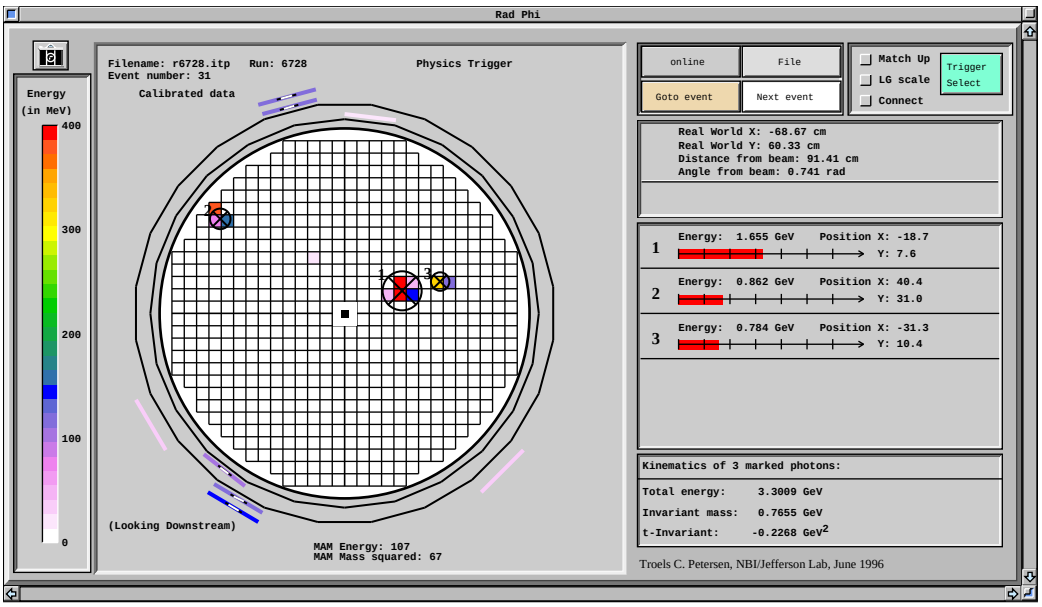

Figure 5.5: The LGD view with the BGV showing three photon clusters in the LGD. The BGV is the outer layer surrounding the LGD.

Chapter 6

Results and Conclusions

6.1 Timing of the Trigger

A study of the timing of the trigger is important for deciding the start time or trigger time, t_0, of each event during a run. The data studied from the high intensity runs during the last three days of the engineering run last summer showed that the σ of the TDC spectra increased to about channel 12.2 on each of the 48 BSD channels which decreased the timing resolution to 6.1 ns. Also present in the TDC spectrum in Figure 6.1 is a double peak which is necessary to understand. In an attempt to understand this behavior, stricter requirements in the analysis were made regarding the tagger. Instead of looking at a coincidence between all of the tagger channels and a BSD channel, plots of a specific tagger channel in coincidence with a BSD channel for each of the BSD channels were created. In Figure 6.1 it can be seen that there is indeed still a double peak and that the spectrum has gotten wider again with σ=7.0ns. Initially, it was thought that this requirement would narrow the TDC spectrum because it would eliminate any variation within the timing of the tagger channels which is not the case when looking at the data. The presence of the double peak in the TDC spectrum signifies that there is more than one element of the trigger setting the start time of an event rather than simply the tagger. Because this TDC

is a common stop ($t = 0$ is the rightmost point), the left peak is being caused by something other than the tagger because its signal is coming after the tagger signal. This leads to the belief that the BSD is occasionally setting the start time, and it is necessary to study and understand the timing of the individual BSD channels.

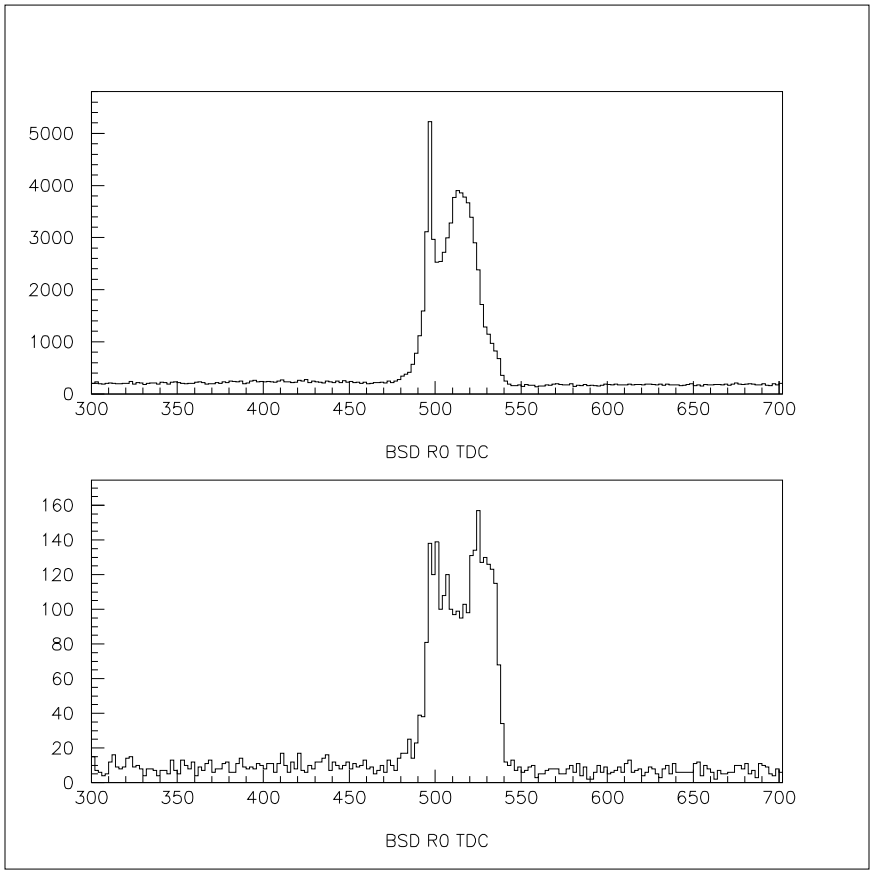

Figure 6.1: The top figure is the TDC spectrum including all tagger channels for a BSD channel. The bottom figure is the TDC spectrum of one tagger channel for a BSD channel.

The cut in the TDC spectra looks at a coincidence between one specific tagger channel and one BSD channel. For each individual BSD channel, the histogram is incremented only if there was a hit in the one tagger channel specified. Once these histograms were generated, Gaussian fits were made to the data to look at the statistics of the distribution. It is expected to see a Gaussian distribution for the TDC

data because the time of an event arrival is a Poisson process. Comparing the σs and means of the histograms with and without the cut, it was observed that the spectra with the tagger cut had an increased σ as well as a shifted mean. Both spectra also included a double peak implying that more than one trigger element was setting the timing. In conclusion, the BSD is setting the timing of the trigger some of the time which indeed would decrease the resolution of the timing since the BSD has several different elements. The reason why the BSD is partially responsible for setting the timing of the trigger can be deduced from the trigger logic (see Figure 4.4). Before the level 1 trigger gets a signal of a triple coincidence in the BSD (a hit in each layer of the BSD), each of the layers of the BSD must be "OR"ed. The signal coming from each of the OR gates must then be "AND"ed. This AND determines whether there is a hit in each layer, each OR must be true. Finally the signal from the AND is sent to the level 1 trigger. Because the BSD signals, must go through all of these gates, it is possible that one BSD channel coming in later than the others can cause the BSD AND to arrive at the level 1 trigger after the tagger and $\overline{UPV}$ despite the design for the tagger signal to be the last to arrive.

At the E94-016 collaboration meeting in December 1999, it was decided that it is unnecessary to determine t_0 for each run of the data. The time of an event in a detector is given by the difference between the time of the hit and t_0. When comparing two elements of a detector or of the experiment, t_0 drops out; and the time is given by the difference between the time of one detector and the time of the second detector.

6.2 BSD Performance

Each of the layers of the BSD are expected to perform equally and similarly well in detecting proton ionization. Because the BSD covers the entire ϕ (azimuthal) direction and the proton has no particular inclination toward a value of ϕ, it is

expected to observe approximately the same number of hits in each layer of the BSD when there is a pixel present. Because there are twice as many straight counters (24) as right (12) or left (12), it is also expected that each of the straight counters will have about half of the occupancy of each of the right or the left counters. Each layer of scintillator in the BSD is only 5 mm thick. For this reason, it is expected that the proton, which is close to minimum ionizing will not stop in any one of the layers, but it will keep moving through to the BGV. As a result, no layer should have any more protons in it than any other layer, and each layer should have approximately equal ionization. In order to confirm that the occupancy of the layers is equal, plots were made for each layer. These histograms were filled as long as there was a hit with an ADC value above channel 100 and a TDC time within the appropriate window. Each histogram shows the number of hits, not only within a layer, but also in each channel of the layer. In this way, the symmetric occupancy in ϕ can also be seen. As seen in Figures 6.3, 6.4, 6.5, this symmetry does not appear to be the case, but is probably a result of poor steering of the beam causing more events to appear at a particular angle in the detector. The straight counters are a direct correlation to the angle in ϕ at which the proton came out of the target (see Figure 6.2). Because the right and left counters cover the same area as the straights, it is still expected that they have similar occupancy (see Figures 6.3, 6.4, 6.5).

Since the voltages on the photomultiplier tubes of the BSD are properly gain-balanced, the peak in the ADC spectra should be in the same place on each of the 48 channels of the BSD. If any of the peaks should move, it is a sign that there is a problem with the hardware of the detector. By looking at the ADC spectra (see Appendix B), it can easily be seen that the ionization peaks are in the same location for all of the detectors which signifies that the hardware seems to be working properly with equal ionization in each layer. In order to do a more rigorous study of

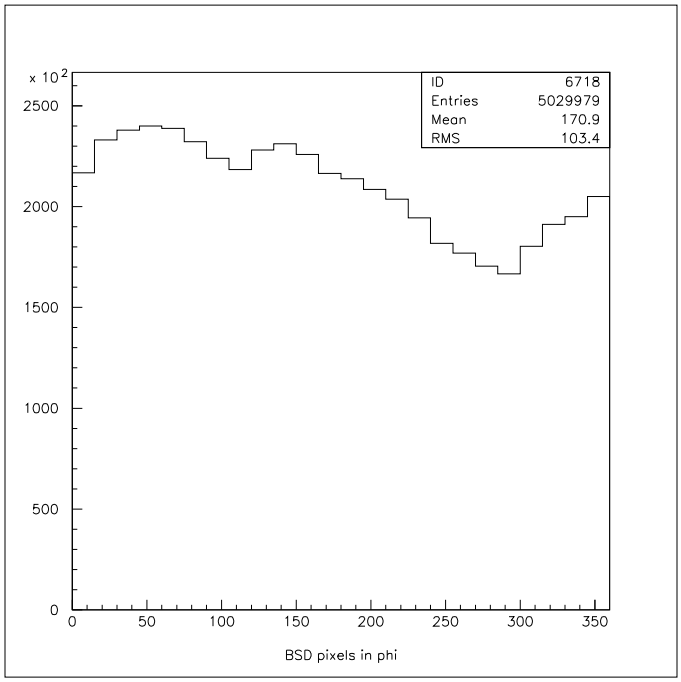

Figure 6.2: The azimuthal angle, ϕ, of the protons.

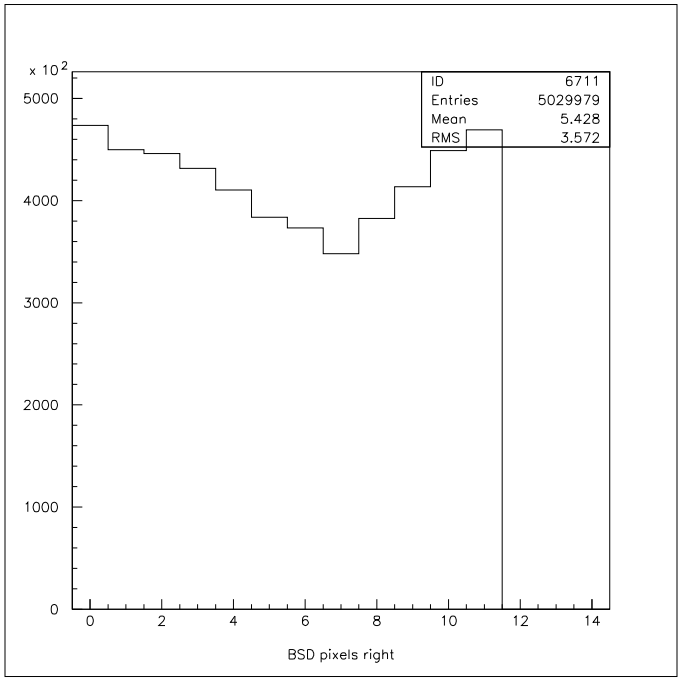

Figure 6.3: The occupancy of the right BSD scintillators.

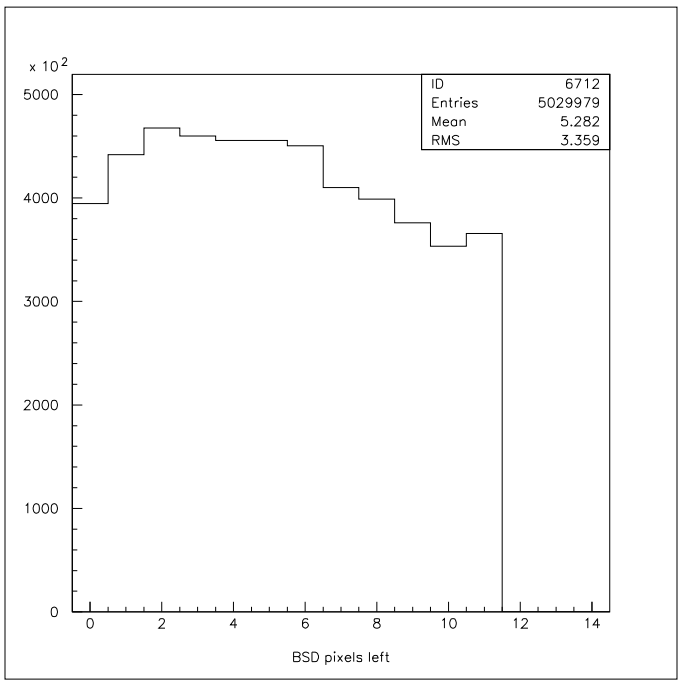

Figure 6.4: The occupancy of the left BSD scintillators.

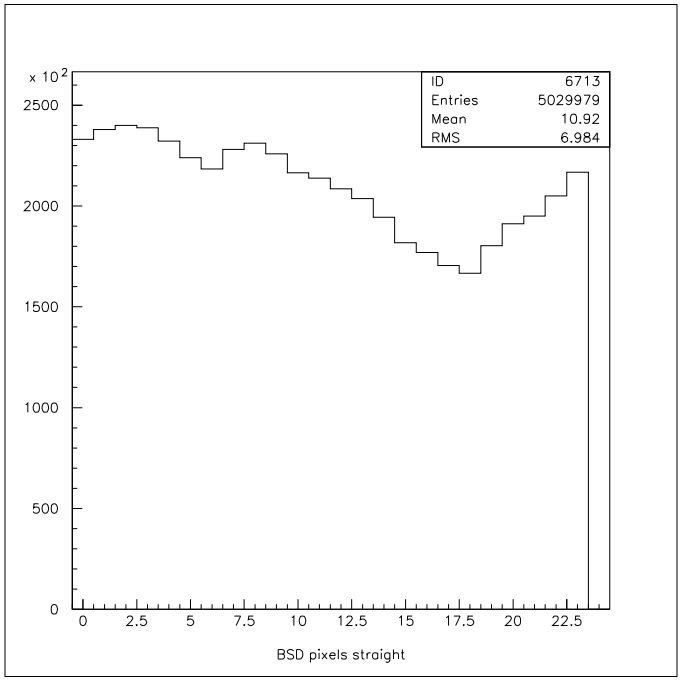

Figure 6.5: The occupancy of the straight BSD scintillators.

the ionization, plots of dE/dx, ionization per layer, were made. Figure 6.6 compares the amount of ionization in the left layer to that in the right layer showing a positive linear relationship between the two layers with the largest concentration of points at 250 channels. Comparing the ionization of the straight counters to the left and right, it is statistically better to average the lefts and rights and compare the result with the straight counters. In Figure 6.7, the same general relationship is seen as in Figure 6.6, but with less variation which signifies a dE/dx closer to one.

6.3 Determination of BSD Hits and Pixels

The majority of time this semester was spent writing code to sort through the raw data in order to create higher level data groups to be used in the analysis by all collaborators. This allows each user to obtain the same definition for certain groups such as hits or coincidences in the detectors. These groups are then created in RODD where the information is sorted through at one time rather than separately in each individual's analysis. Groups are defined for hits and pixels in the BSD by sorting through the raw ADC and TDC information.

The group of "BSD hits" defines a hit as having an ADC value above a particular threshold and as having a TDC hit within a specified time window. The code for this determination is found in Appendix A. The first step in the process of defining the BSD hits group (in essence, a C structure) is to loop through the ADC values for each channel and subtract the pedestal from each value. This value is then recorded as the new ADC value or ionization value for each channel. Once this is done, the next step is to loop through all of the TDC values for each channel and convert the time in channels to a time in nanoseconds by multiplying by a factor of 0.5. Then the absolute value of the difference between the time and relative t_0 is taken and checked to be within a certain time window, Δt. Because the TDC is a multihit

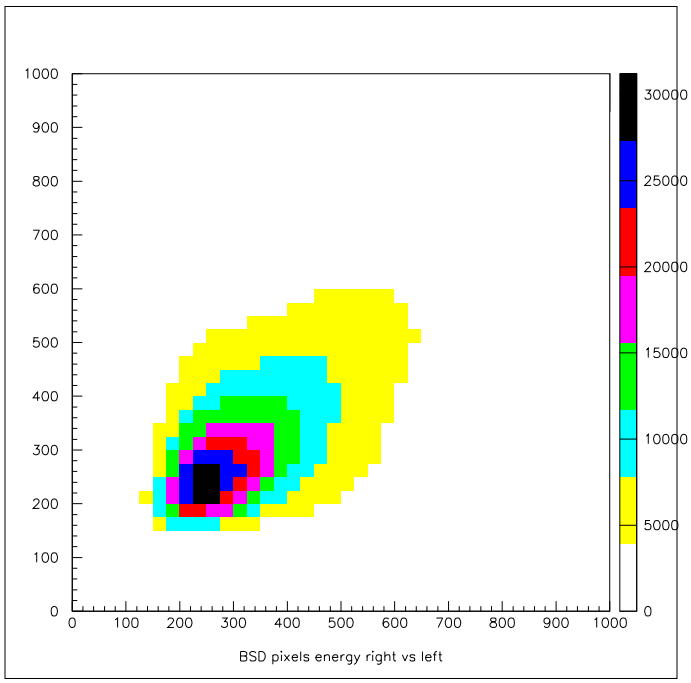

Figure 6.6: Correlation between dE/dx measured for the right and left layers.

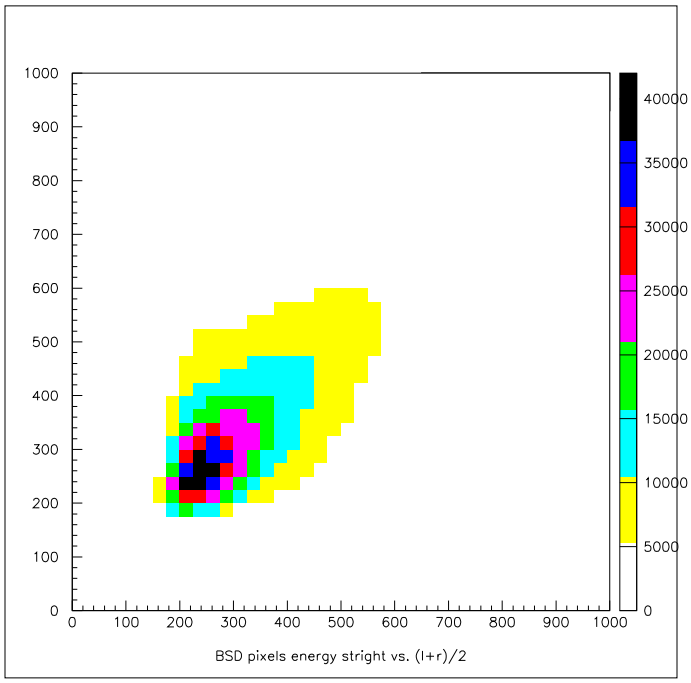

Figure 6.7: Correlation between dE/dx measured for the straight vs. (R+L)/2.

TDC, there can exist more than one time for a particular channel. For this reason, the time is recorded in an array for each channel and the index of the different times for each channel is incremented. The final step in forming the BSD hits struct is to loop through each of the 48 BSD channels and check to see that the ADC value is above a certain threshold and that the channel has at least one TDC hit. If these conditions hold, the BSD channel is considered to have a hit; therefore, the channel number, the ADC value, the index of times, and the array of times are written to the "BSD hits" group. After each true hit, the number of hits is incremented; and the process continues until all events have been processed.

The group of "BSD pixels" defines a pixel as an overlapping region of a right, left, and straight scintillator in which each scintillator has a correctly defined hit. In order to define this pixel, the channel numbers of the BSD (0-47) must be converted into right (R0-R11), left (L0-L11), and straight (S0-S23) channel numbers. This first step requires looping through the number of BSD hits and checking the channel number. If the channel number is 0-11, the channel is recorded in an array of right channels with the original BSD channel number. Separately, the energy (ADC value) is recorded in an energy array for these right channels. Similarly, if the BSD channel number is 12-23 or 24-47, the channel number is recorded in an array for lefts or straights with the BSD channel minus 12 or 24 respectively. The energies are also recorded as separate energy arrays for the lefts and straights. After each of these steps, the number of rights, lefts, and straights is incremented until each array is full. Once this step is completed, all combinations of the right, left, and straight counters are looped through in order to find all possible pixels. Each combination of R,L, and S channel numbers is fed into a function where it can be determined whether or not the combination actually forms a pixel in the hardware. The function returns a nonnegative number (the ring number) describing the pixel's position in

z if it is a pixel or -1 if it is not an actual pixel. If this value is nonnegative, the information written to the BSD pixel struct includes the R, L, and S channel numbers and their corresponding energy values along with the ring number and position in ϕ (corresponding to the straight counter of the BSD). After all of this is recorded, the number of pixels is incremented in order to define the number of pixels per event. Finally, the groups of hits and pixels of the BSD are defined with all of their relevant data recorded.

6.4 Reconstruction of the ω Meson in the LGD

Reconstruction of the ω meson in the LGD provides a check of how the detector works. Because the acceptance of the radiative ϕ decays is lower than the ω acceptance, it is appropriate to check what it is necessary to do in order to determine the ω mass clearly before trying to reconstruct the ϕ meson. The invariant mass or "rest mass" of a particle is given by

$$p^2 = E^2 - \vec{p}^{\,2} \equiv M^2, \tag{6.1}$$

where p is the 4-vector of the momentum, E is the energy, and $\vec{p}$ is the 3-momentum of the particle. For a photon,

$$E^2 - \vec{p}^{\,2} = 0; \tag{6.2}$$

therefore, the two photon effective mass is given by

$$M^2 = (p_1 + p_2)^2 \tag{6.3}$$

$$= 2E_1E_2 - 2\vec{p_1} \cdot \vec{p_2} \tag{6.4}$$

$$M^2 = 2E_1E_2(1 - \cos\theta) \tag{6.5}$$

where θ is the angle between the two photons. Similarly, this can be calculated to find the three photon effective mass. The two photon invariant mass shown in figure 6.8

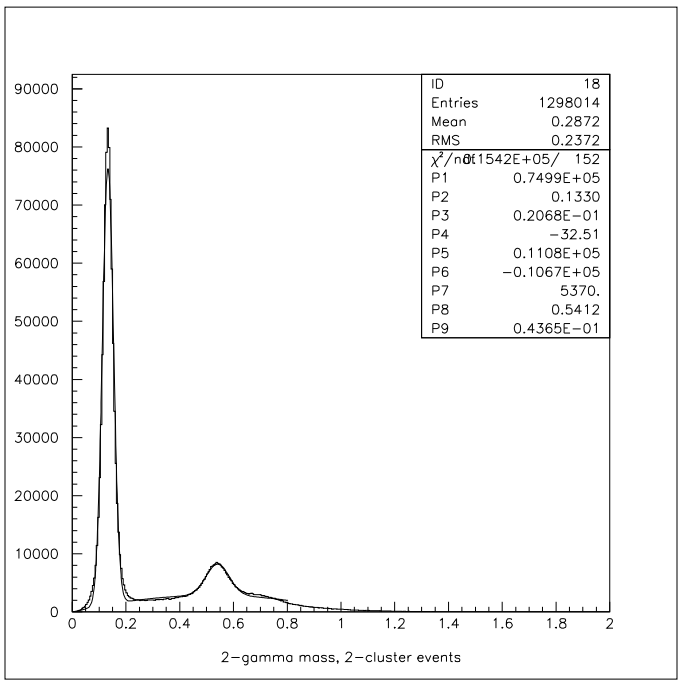

Figure 6.8: Two photon effective mass (in GeV) with a Gaussian fit superimposed showing the π^0 mass at 133 MeV and the η mass at 541 MeV.

clearly displays the π^0 resonance peak (mass spectrum) at approximately 0.133 GeV, compared to the actual mass of 0.135 GeV, and the η resonance peak at approximately 0.541 GeV, compared to the actual mass of 0.547 GeV.

In the analysis of the decay $\omega \rightarrow \pi^0\gamma$, the three photon invariant mass is determined in a couple of different ways. The invariant mass of the ω is determined by calculating the three photon invariant mass (Figure 6.9) or by calculating the invariant mass of the π^0 and then adding the invariant mass of the third photon in the LGD (Figure 6.10). The ω resonance peak starts to become visible at this point, but it is not well defined. When looking at the three photon effective mass without a π^0, the π^0 peak becomes more prominent and a spectrum around the ω is still seen (see Figure 6.11). The fact that the π^0 mass is visible when looking at the three photon invariant mass implies that the clusterizer is categorizing some two photon π^0

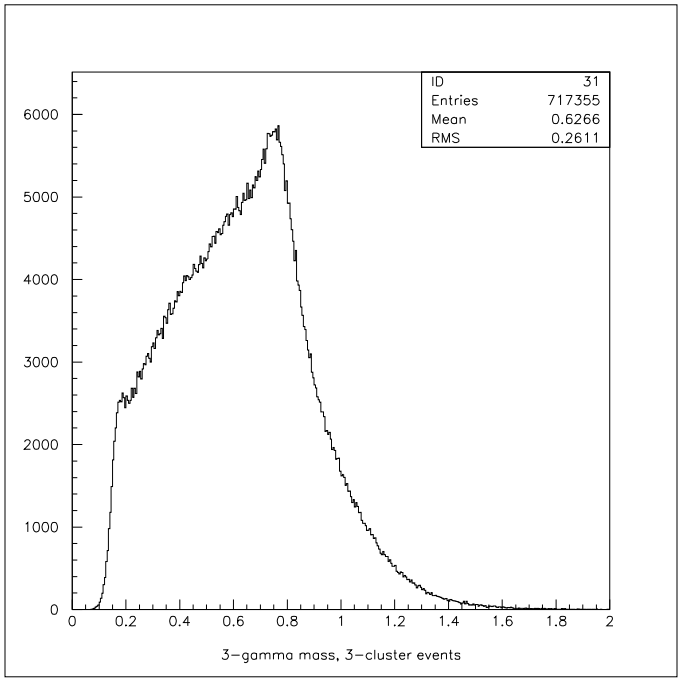

Figure 6.9: Three photon effective mass.

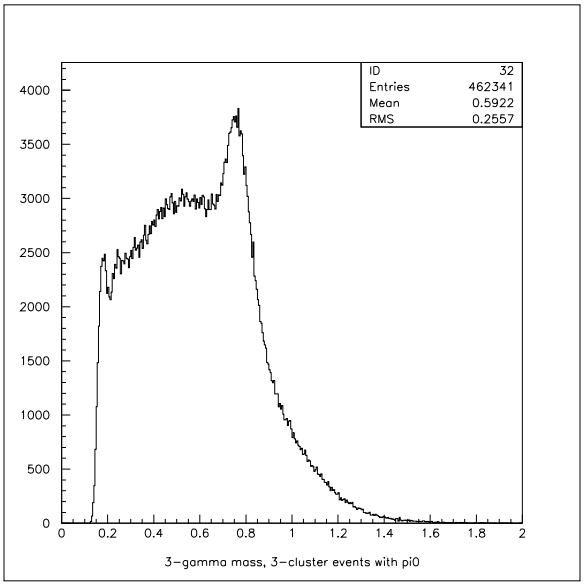

Figure 6.10: Three photon effective mass with π^0 criterion.

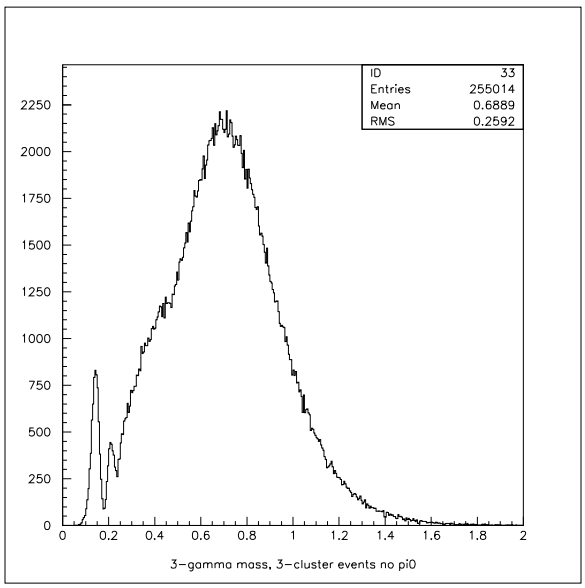

Figure 6.11: Three photon effective mass without π^0 criterion.

events as three photon events. This clusterizing problem needs to be studied further, especially for data analysis reconstructing five photon events such as the f_0 and the a_0.

More stringent cuts are made on the energies of the photons in the LGD as well as the total energy allowed in the LGD in order to identify the ω mass more carefully. The first cut requires that each photon in the LGD be at an energy of at least 500 MeV. Then the three photon invariant mass is plotted with a π^0 present (see Figure 6.12), without a π^0 present (see Figure 6.13), and simply the three photon effective mass (see Figure 6.14). The second, separate cut made requires an energy of at least 4 GeV in the LGD, since the photons interacting with the target are no less than 4.25 GeV. The same three plots are made in this case as well (see Figures 6.15, 6.16, 6.17 respectively). The next step in defining the ω mass spectrum clearly is requiring that each photon in the LGD have energy of at least 500 MeV along with the 4 GeV stipulation on the LGD. In this case, when the three photon effective mass is plotted

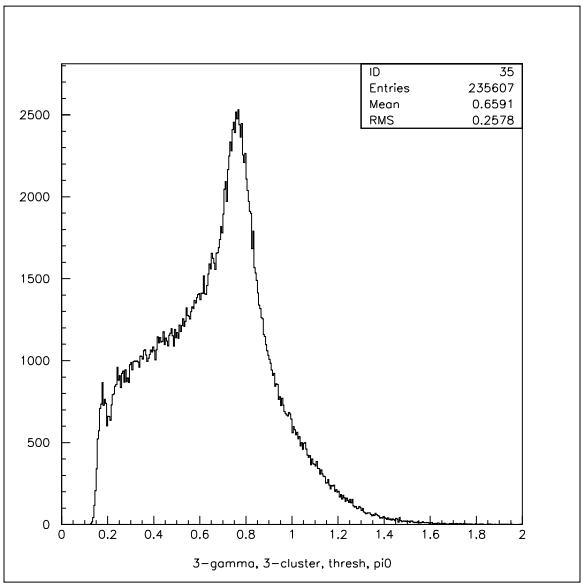

Figure 6.12: Three photon effective mass with threshold cut and π^0 criterion.

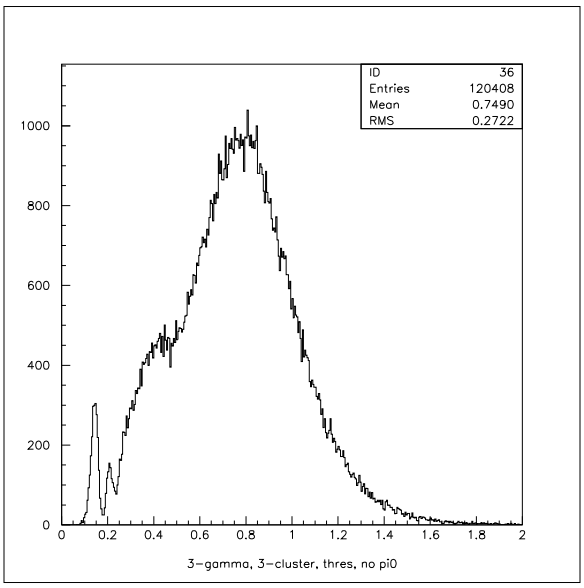

Figure 6.13: Three photon effective mass with threshold cut and no π^0.

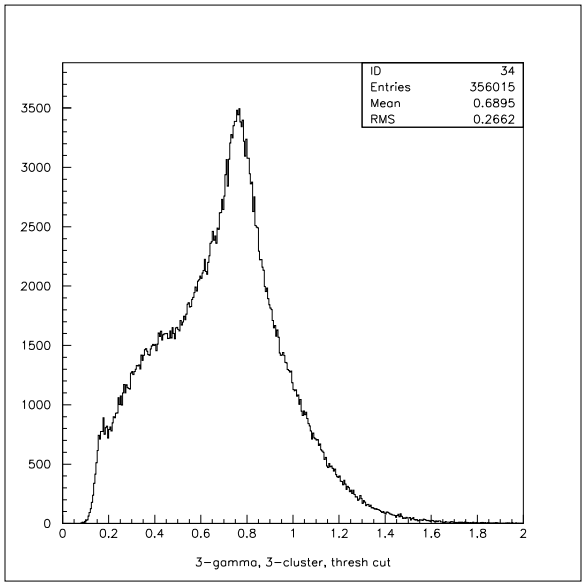

Figure 6.14: Three photon effective mass with threshold cut.

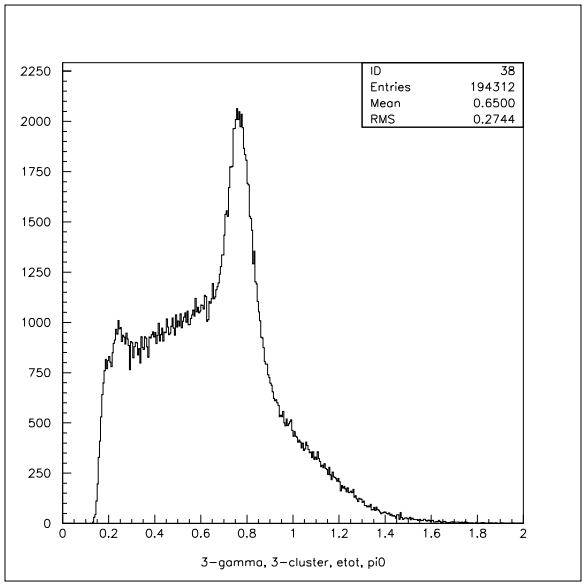

Figure 6.15: Three photon effective mass with threshold cut, total energy cut, and π^0 criterion.

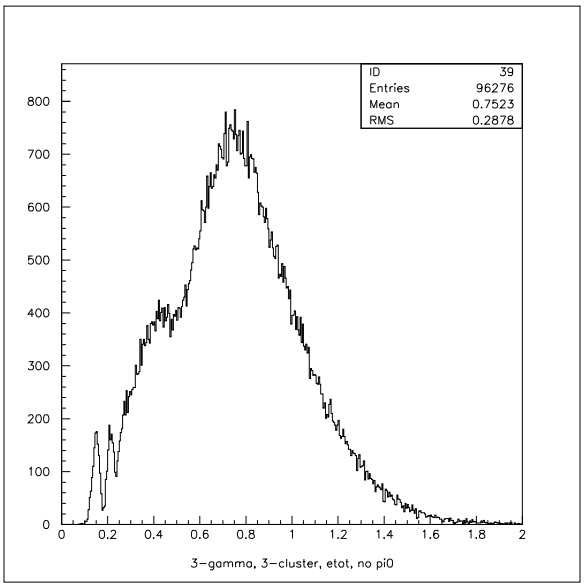

Figure 6.16: Three photon effective mass with total energy cut and no π^0.

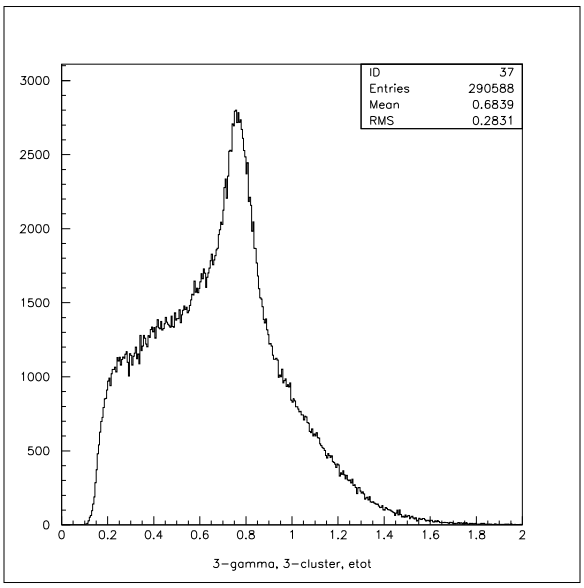

Figure 6.17: Three photon effective mass with the total energy cut.

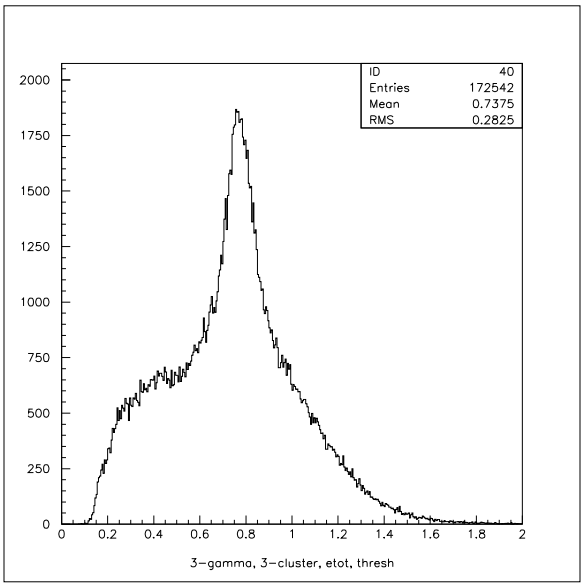

Figure 6.18: Three photon effective mass with threshold cut and total energy cut.

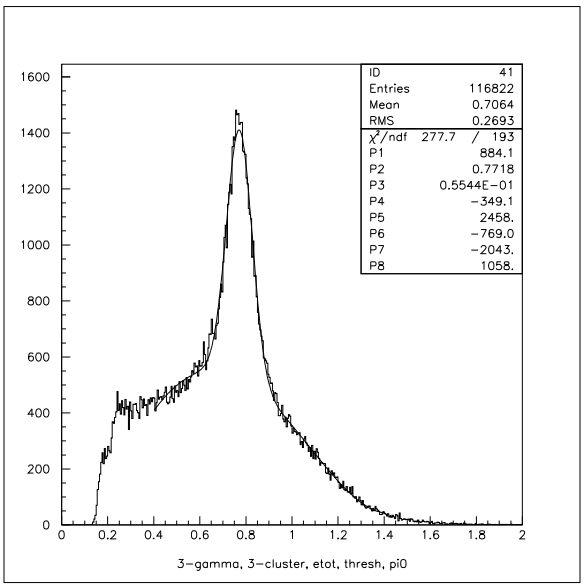

Figure 6.19: Three photon effective mass with threshold cut, total energy cut, and π^0 criterion. A Gaussian fit is superimposed with a mean value of 772 MeV.

the ω mass becomes very clear see figure 6.18. Figure 6.19 requires that there be a π^0 in the LGD. In this case, the ω resonance narrows quite a bit and is clearly recognizable at approximately 0.772 GeV when the actual mass sits around 0.782 GeV.

These requirements in the LGD and reconstruction of photons in the LGD clearly show that it is possible to identify many-photon events with the given statistics. The next step in the analysis is to consider the anticorrelation of the momentum between the ω and the proton.

6.5 Proton and ω Meson Momenta

The radial momentum vectors of the proton and ω meson should add to zero since the proton starts at rest in the Be target. Once the anticorrelation is identified, a more stringent cut can be made on the ω plots in order to refine the resolution of the ω resonance. The correlation also indicates that the experimental setup is working as expected, which is essential to properly detect rarer decays such as those of the ϕ meson.

In order to determine the radial momentum of the proton, the straight counter through which the proton traversed is converted to the azimuthal angle. This is done simply by looking at the geometry of the detector. Because there are 24 scintillators covering the azimuthal angle of the BSD, each one corresponds to a range of 15°. The S0 counter corresponds to the range $\phi = 15° - 30°$, and the S23 counter corresponds to the range $\phi = 0° - 15°$; therefore the entire azimuthal angle is covered.

For each photon in the lead glass, the x, y, and z components of its momentum are known; therefore the angle ϕ can be calculated for the photon. Because the anticorrelation is being studied for the proton and the ω meson, and not individual photons, the angle ϕ is calculated for the ω rather than each of the decay photons.

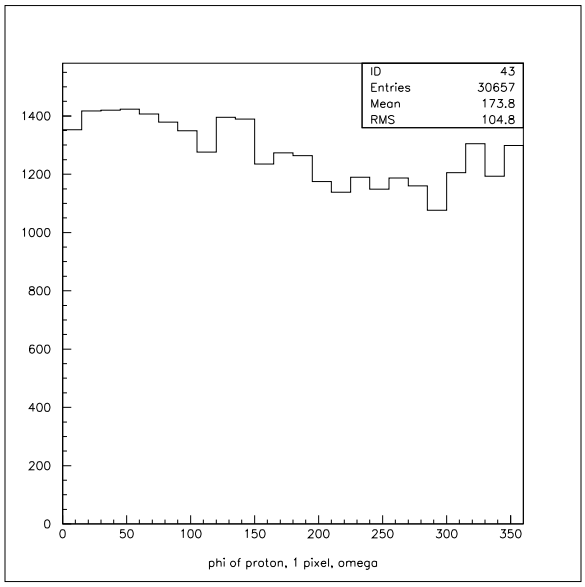

Figure 6.20: The azimuthal angle of the proton momentum.

The process of determining the azimuthal angle of the ω meson is only done for a defined ω mass window and as long as there was only one pixel in the BSD. The x-coordinate of each of the three photons is added together in order to get p_x for the ω meson. Similarly, this is done for the y-coordinate. Once the x- and y-coordinates of the ω meson are determined, the arctangent of y/x is calculated as $-\pi \leq \phi \leq \pi$. The arctangent is converted to degrees by multiplying by the appropriate scaling factor; and if the value of the arctangent is negative, 360° is added to its value so that $0° \leq \phi \leq 360°$. The plots of the proton and ω meson azimuthal angle are seen in Figures 6.20 and 6.21 respectively. The distribution of these particles momenta in ϕ are uniform; as expected they favor no ϕ angle.

The anticorrelation of the proton and ω momenta is explored by looking at a plot with the azimuthal angle of the proton against that of the ω meson. A direct linear relationship between the angle of the momenta is seen in figure 6.22. The plot clearly shows a slope of one and an x- and y-intercept of 180° corresponding the anticorrelation of the proton and ω momenta. The difference between the proton

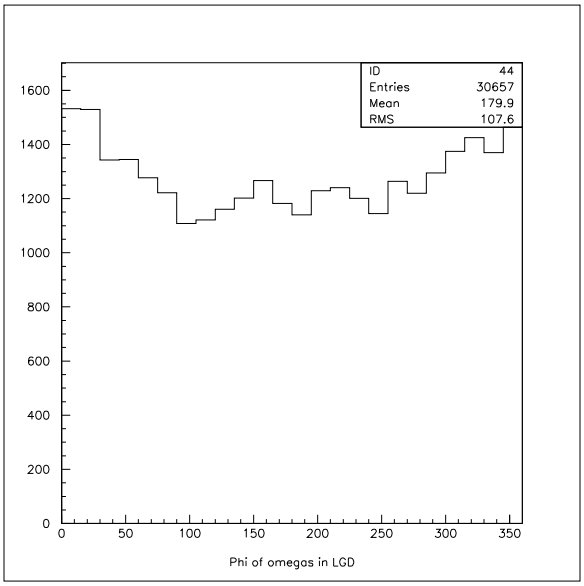

Figure 6.21: The azimuthal angle of the ω meson momentum.

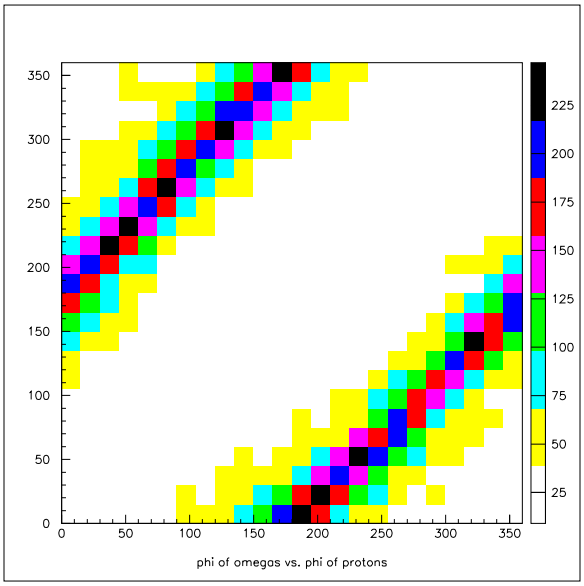

Figure 6.22: The azimuthal angle of the proton momentum plotted against that of the ω meson.

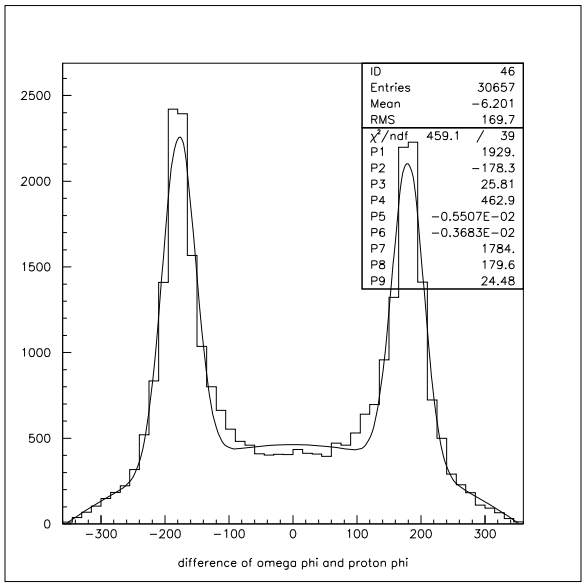

Figure 6.23: The difference of the azimuthal angle of the proton and ω momenta.

momentum and the ω momentum is shown in figure 6.23. The difference plot clearly shows two peaks at $-180°$ and $180°$. There are two peaks in this plot because the absolute value of the difference was not taken into consideration. In order for these two particles to conserve momentum, it is expected that their difference would be $180°$; therefore, the plot shows that our detectors are working properly and the the necessary information from the detectors is being recorded.

Now it has been proven that the process $\omega \to \pi^0\gamma$ can be detected properly, the next step in the analysis is to make stricter cuts on the BSD information. This enables more selective requirements for a hit, therefore a pixel, in the BSD. The result desired would be to see an even greater reduction in the background events so that a mass resonance peak is better defined. This will be tested initially using the process $\omega \to \pi^0\gamma$. Because this selection will be much more important when looking at processes such as $\phi \to a_0\gamma$ and $\phi \to f_0\gamma$ which have much lower acceptance than the ω decay, it is important to determine whether these more stringent cuts will make a difference in identifying mass resonances.

6.6 Conclusions and Future Plans

Several different aspects of the BSD were studied this year. It was determined that t_0 does not need to be determined because differences can be taken between times of detector elements in order to determine the timing of an event. The layers of the BSD seem to work as expected with occupancy of each of the layers to be uniformly distributed and dE/dx is consistent between the layers. Consistent dE/dx between the layers implies that the proton is in fact ionizing evenly in each of the layers of the BSD as predicted. BSD hits and pixels can be identified from the ADC and TDC information providing more in-depth analysis. The ω meson mass was identified and will be used to calibrate cuts to identify other particles. The correlation of the proton and the ω meson was observed so the BSD can be used as a valid trigger element and can be used to efficiently select good events. Identifying the ω meson as well as the correlation with the proton is extremely important because it will be much more difficult to identify the a_0 and the f_0 which are reconstructed from five photon events. The cuts made from the momentum correlation will cut out the background and make the mass resonances more clearly identifiable.

The future plans for the project include making more stringent cuts on the BSD in order to decrease the width of the mass spectrum of reconstructed particles such as the ω. These cuts are useful in order to improve the signal to background, which will in turn improve the identification of mass resonances. The "hits" group needs to be defined for the other detectors for use in the analysis to improve the identification of particles. Other decay modes also need to be studied in the analysis. Beginning in May 2000, three months of high-rate data will be taken to further these studies and to determine the nature of the $f_0(980)$ and $a_0(980)$ mesons.

Appendix A

Functions Defining BSD Hits and Pixels

A.1 BSD Hits

The following is the C code which fills the BSD hits struct.

```
/************************** makeBSDHits ******************************/

/*   Lisa Kaufman   */

int makeBSDHits(itape_header_t *event, time_list_t *timeList)
{
#define nBSDChannels 48  /*corresponds to the number of scintillators of the BSD*/
  adc_values_t *bsd=NULL;
  tdc_values_t *tbsd=NULL;
  static bsd_hits_t *bsdHits=NULL;
  static bsd_hits_t *tmp=NULL;
  int i,j,k,m;
  int size;
  float bsdped = 0.0; /*corresponds to bsd pedestal for a channel*/
  float bsdadctoenergy = 1; /*converts bsd adc to ionization energy*/
  float channeltotime = 0.5; /*converts channel of time to time in ns*/
  float bsdthresh =  100.0; /* threshold for the ADC signal for a good hit*/
  float deltat = 25;
  float tzero = 250;

  int adcValue[nBSDChannels];
  int ntdchits[nBSDChannels];

  struct bsdtimes{
    int ntimes;
    int tdctimes[16];
  };

  struct bsdtimes tdcValue[nBSDChannels];
```

```
  /* bsdped = 0;  should be an array of form malloc(nBSDChannels*sizeof(float))
  bsdadctoenergy = 1;  should be an array: malloc(nBSDChannels*sizeof(float))

  channeltotime = 0.5;  should be array?
  bsdthresh = 0. */

  for(i=0; i < nBSDChannels; i++){
    adcValue[i]=0;
  }
  for(i=0; i < nBSDChannels; i++){
    ntdchits[i]=0;
  }

  for(i=0; i < nBSDChannels; i++){
    tdcValue[i].ntimes=0;
    for(j=0; j < 16; j++){
      tdcValue[i].tdctimes[j]=0;
    }
  }

  if(bsdHits==NULL){
    bsdHits = malloc(sizeof(adc_hits_t)*(nBSDChannels)*sizeof(adc_hit_t));
  }

  bsdHits->nhits = 0;

  if((bsd = data_getGroup(event,GROUP_BSD_ADCS,NULL)) == NULL){
    fprintf(stderr,"No BSD ADCs\n");
    return(1);
  }

  if ((tbsd = data_getGroup(event,GROUP_BSD_TDCS_LONG,NULL)) == NULL){
    fprintf(stderr,"No BSD TDCs\n");
    return(1);
  }

  for(i=0; i < bsd->nadc; i++){
    adcValue[bsd->adc[i].channel] = (bsd->adc[i].value - bsdped)*bsdadctoenergy;
         /*should be bsdped[bsd->adc[i].channel*/
  }

  for(j=0; j < tbsd->ntdc; j++){
    if(abs((((tbsd->tdc[j].le)*channeltotime) - tzero)) < deltat){
      if (tbsd->tdc[j].channel < nBSDChannels){   /* added dsa */
tdcValue[tbsd->tdc[j].channel].tdctimes[ntdchits[tbsd->tdc[j].channel]]
 = (tbsd->tdc[j].le)*channeltotime;
ntdchits[tbsd->tdc[j].channel]++;
tdcValue[tbsd->tdc[j].channel].ntimes = ntdchits[tbsd->tdc[j].channel];
      }
```

```
    }
  }


  for(k=0; k < nBSDChannels; k++){
    if((adcValue[k] > bsdthresh) && (tdcValue[k].ntimes > 0)){

      bsdHits->hit[bsdHits->nhits].channel = k;
      bsdHits->hit[bsdHits->nhits].energy = adcValue[k];
      bsdHits->hit[bsdHits->nhits].times = tdcValue[k].ntimes;
      for(m=0; m < tdcValue[k].ntimes; m++){
bsdHits->hit[bsdHits->nhits].tindex = timeList->nelements;
timeList->element[bsdHits->hit[bsdHits->nhits].tindex].le =
tdcValue[k].tdctimes[m];
timeList->nelements++;
      }
      bsdHits->nhits++;
    }
  }
  if (bsdHits->nhits){
    size = sizeof(bsd_hits_t) + (bsdHits->nhits)*sizeof(bsd_hit_t);
  }
  else {
    size = sizeof(bsd_hits_t);
  }
  tmp = data_addGroup(event,100000, GROUP_BSD_HITS,NULL,size);
  memcpy(tmp,bsdHits,size);
  free(bsdHits);
  bsdHits=NULL;

  return(0);
}
```

A.2 BSD Pixels

The following is the C code which fills the BSD pixels struct along with the algorithm which defines a pixel in the hardware.

```
/*****************************makeBSDPixels*******************/

/*   Lisa Kaufman   */

int makeBSDPixels(itape_header_t *event)
{
  bsd_hits_t *bsdHit=NULL;
  static bsd_pixels_t *bsdPixels=NULL;
  static bsd_pixels_t *tmp=NULL;
  int i=0;
  int size;
  int nright=0;
```

```
int nleft=0;
int nstraight=0;
int R,L,S = 0;
int bsdring = PIXEL_Z_INVALID;
int right[12];
int left[12];
int straight[24];
float energy_r[12];
float energy_l[12];
float energy_s[24];

for(i=0; i<12; i++){
  right[i]=0;
  energy_r[i]=0;
  left[i]=0;
  energy_l[i]=0;
}

for(i=0; i<24; i++){
  straight[i]=0;
  energy_s[i]=0;
}

if(bsdPixels==NULL){
  bsdPixels = malloc(sizeof(bsd_pixels_t)*sizeof(bsd_pixel_t)*(nBSDChannels));
}

bsdPixels->npixels = 0;

if((bsdHit = data_getGroup(event,GROUP_BSD_HITS,NULL)) == NULL){
  fprintf(stderr,"No BSD Hits\n");
  return(1);
}

for(i=0; i < bsdHit->nhits; i++){
  if((bsdHit->hit[i].channel >= 0) && (bsdHit->hit[i].channel < 12)){
    right[nright]=bsdHit->hit[i].channel;
    energy_r[nright] = bsdHit->hit[i].energy;
    nright++;
  }
  else if((bsdHit->hit[i].channel >=12) && (bsdHit->hit[i].channel < 24)){

    left[nleft]=(bsdHit->hit[i].channel) - 12;
    energy_l[nleft] = bsdHit->hit[i].energy;
    nleft++;
  }
  else {
    straight[nstraight]=(bsdHit->hit[i].channel) - 24;
    energy_s[nstraight] = bsdHit->hit[i].energy;
    nstraight++;
  }
```

```
  }

  for(R=0; R<nright; R++){
    for(L=0; L<nleft; L++){
      for(S=0; S<nstraight; S++){
bsdring=get_pixel_Z_from_RLS(right[R],left[L],straight[S]);
if(bsdring != (PIXEL_Z_INVALID)){
  bsdPixels->pixel[bsdPixels->npixels].right = right[R];
  bsdPixels->pixel[bsdPixels->npixels].left = left[L];
  bsdPixels->pixel[bsdPixels->npixels].straight = straight[S];
  bsdPixels->pixel[bsdPixels->npixels].energy[0] = energy_r[R];
  bsdPixels->pixel[bsdPixels->npixels].energy[1] = energy_l[L];
  bsdPixels->pixel[bsdPixels->npixels].energy[2] = energy_s[S];
  bsdPixels->pixel[bsdPixels->npixels].ring=bsdring;
  /* bsdPixels->pixel[bsdPixels->npixels].z =;*/
  if(straight[S] == 23){
    bsdPixels->pixel[bsdPixels->npixels].phi = 7.5;}
  else{
    bsdPixels->pixel[bsdPixels->npixels].phi = 22.5 + (15.0 * straight[S]);
  }
  bsdPixels->npixels++;
}
      }
    }
  }

  if(bsdPixels->npixels)
    size = sizeof(bsd_pixels_t) + (bsdPixels->npixels-1)*sizeof(bsd_pixel_t);
  else
    size = sizeof(bsd_pixels_t);
  tmp = data_addGroup(event,100000,GROUP_BSD_PIXELS,NULL,size);
  memcpy(tmp,bsdPixels,size);
  free(bsdPixels);
  bsdPixels=NULL;

  return(0);
}

/************************************ get_pixel_z ************************/

/*   Lisa Kaufman   */

int get_pixel_Z_from_RLS(int R, int L, int S)
{
  int Z,test_S;
  Z=L-R;
  if(Z<0) /* staying within the proper domain */
    Z+=12;
  if(Z>=12)
    Z-=12;
```

```
  test_S=L+R;
  if(R>L) /* again... */
    if(test_S<12)
      test_S+=12;
    else
      test_S-=12;

  if(Z<9 && (S==test_S || S==((test_S+1)%24)) )
    return Z;
  else
    return PIXEL_Z_INVALID;
}
```

Appendix B

ADC Spectra of the BSD

The BSD ADC spectra are plotted below on a logarithmic scale where the minimum ionizing peak can be seen approximately at channel 250.

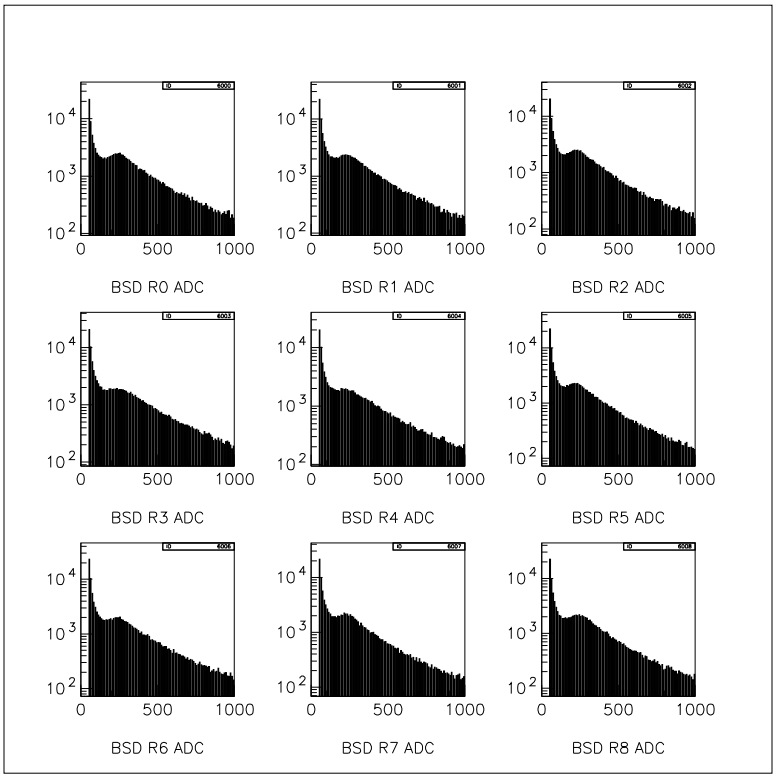

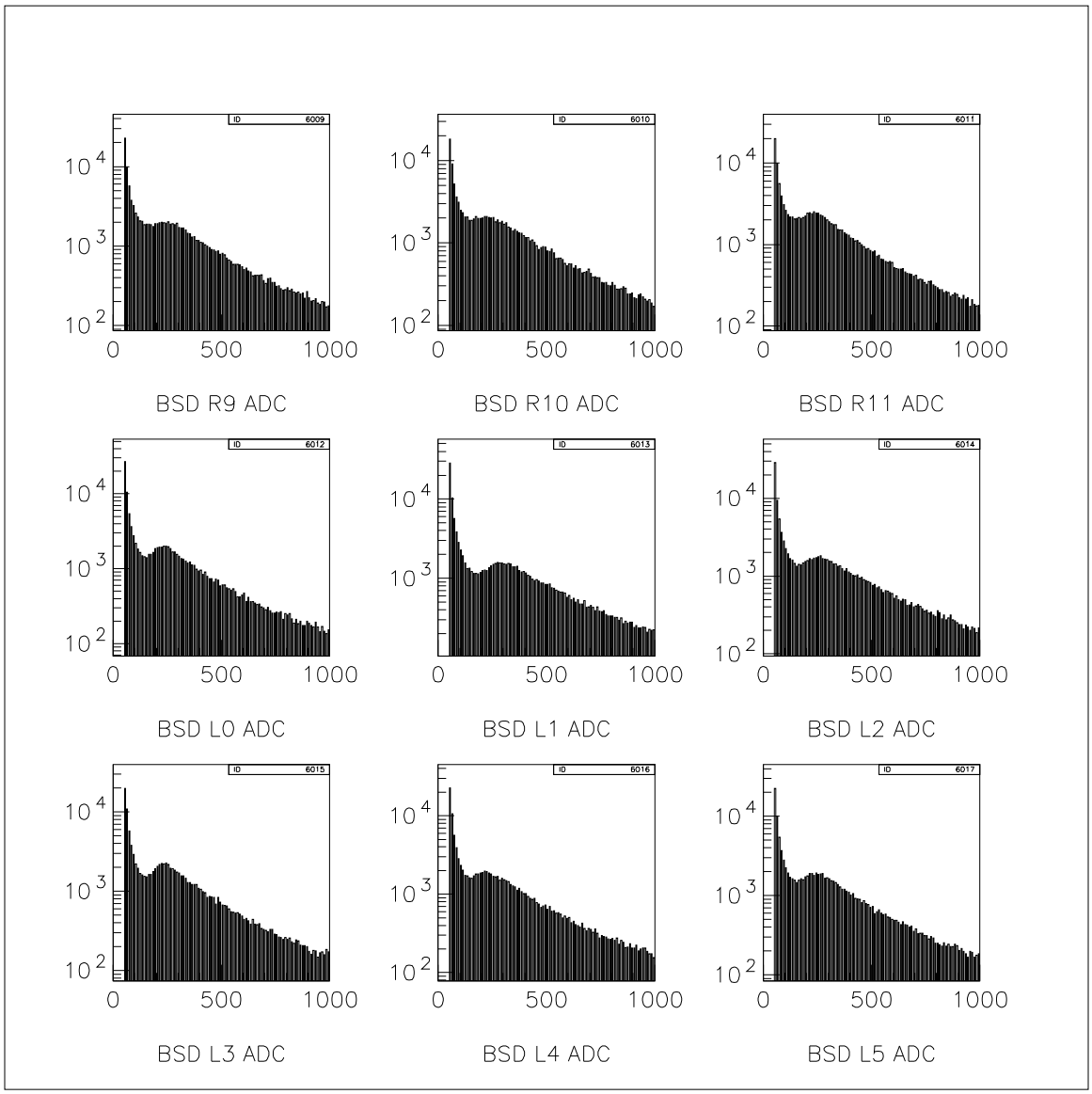
ID 6009
BSD R9 ADC
ID 6010
BSD R10 ADC
ID 6011
BSD R11 ADC
ID 6012
BSD L0 ADC
ID 6013
BSD L1 ADC
ID 6014
BSD L2 ADC
ID 6015
BSD L3 ADC
ID 6016
BSD L4 ADC
ID 6017
BSD L5 ADC
0
500
1000

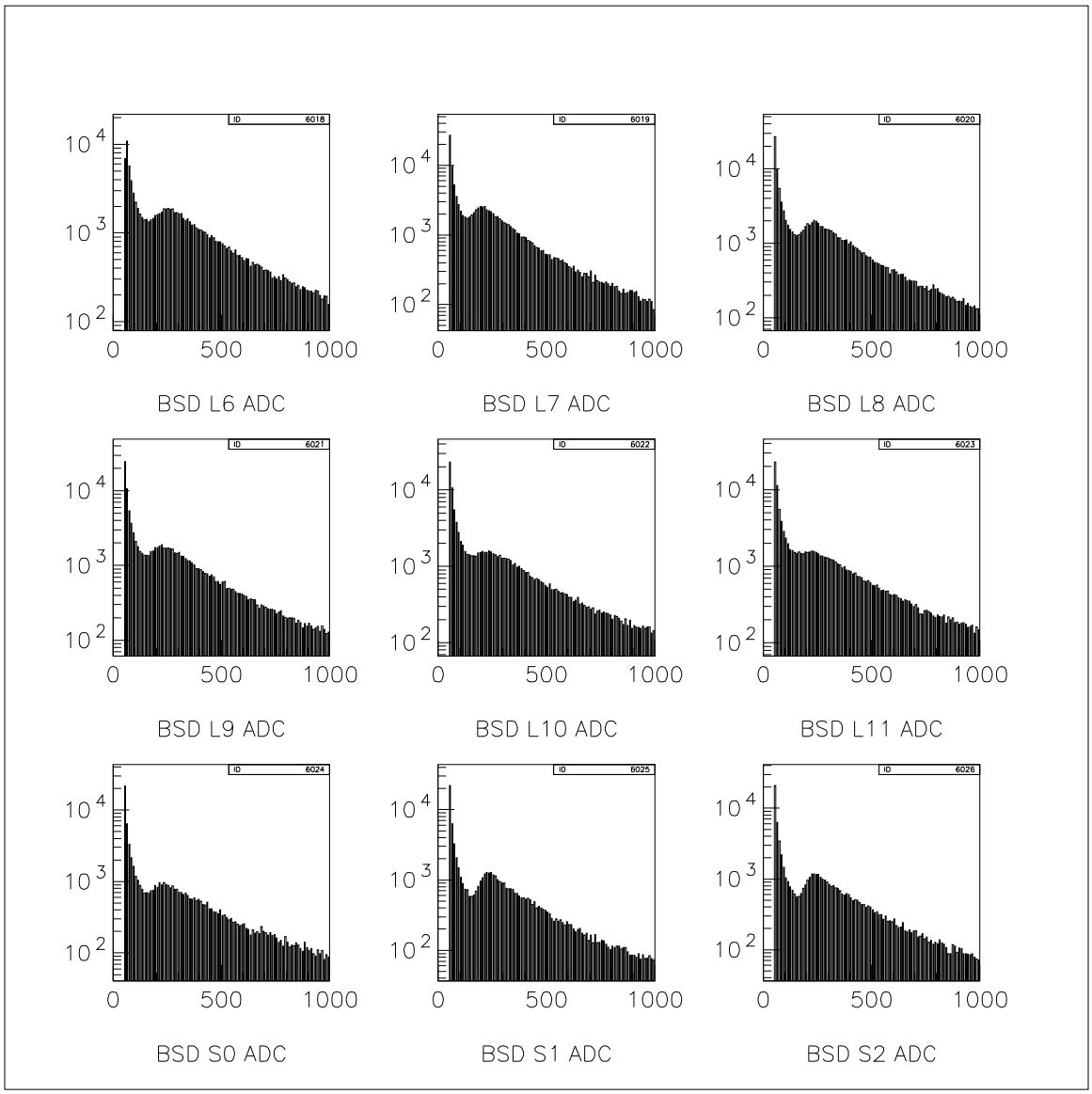
ID 6018
BSD L6 ADC
ID 6019
BSD L7 ADC
ID 6020
BSD L8 ADC
ID 6021
BSD L9 ADC
ID 6022
BSD L10 ADC
ID 6023
BSD L11 ADC
ID 6024
BSD S0 ADC
ID 6025
BSD S1 ADC
ID 6026
BSD S2 ADC
0
500
1000

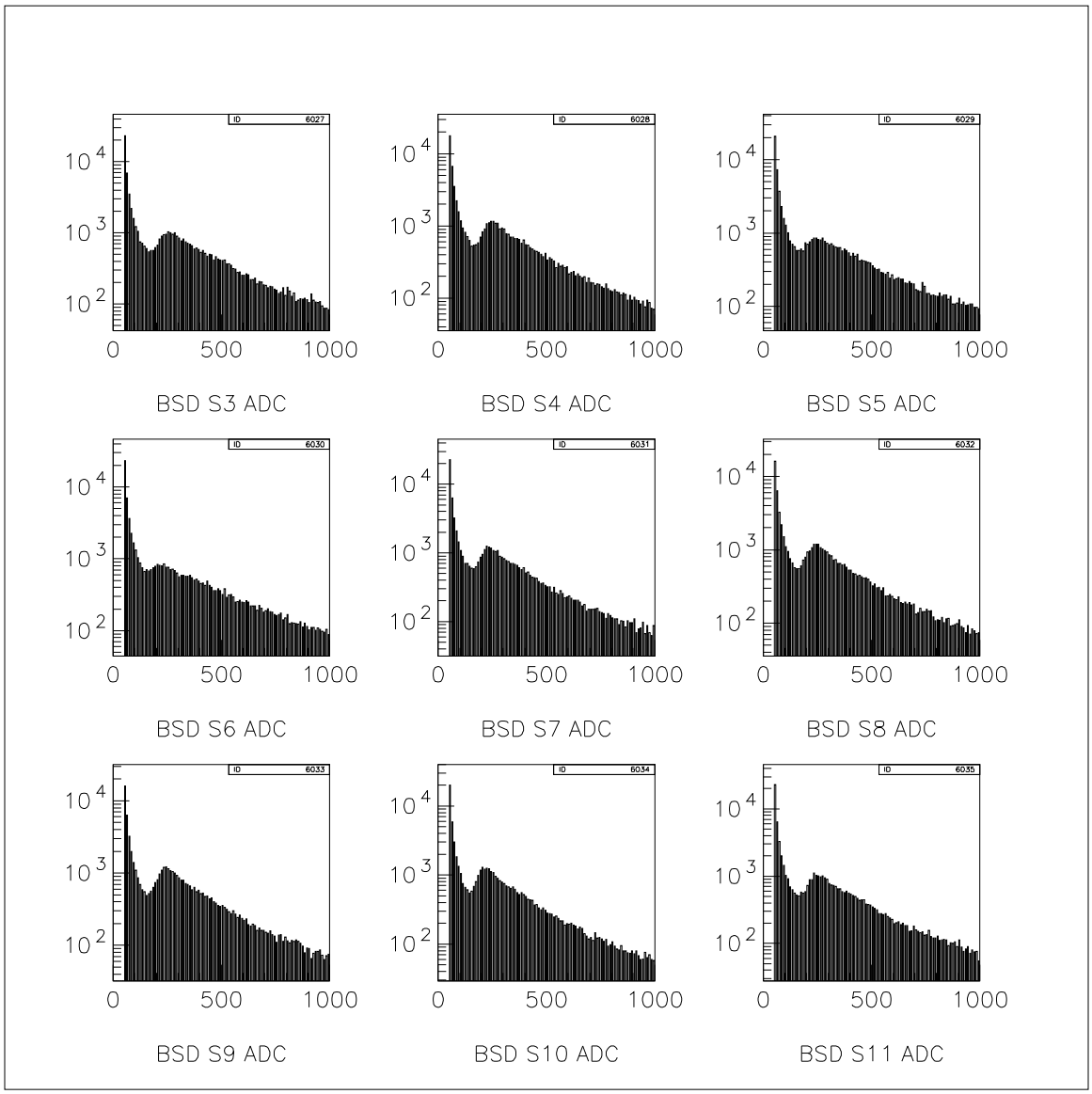
ID 6027
BSD S3 ADC
ID 6028
BSD S4 ADC
ID 6029
BSD S5 ADC
ID 6030
BSD S6 ADC
ID 6031
BSD S7 ADC
ID 6032
BSD S8 ADC
ID 6033
BSD S9 ADC
ID 6034
BSD S10 ADC
ID 6035
BSD S11 ADC
0
500
1000

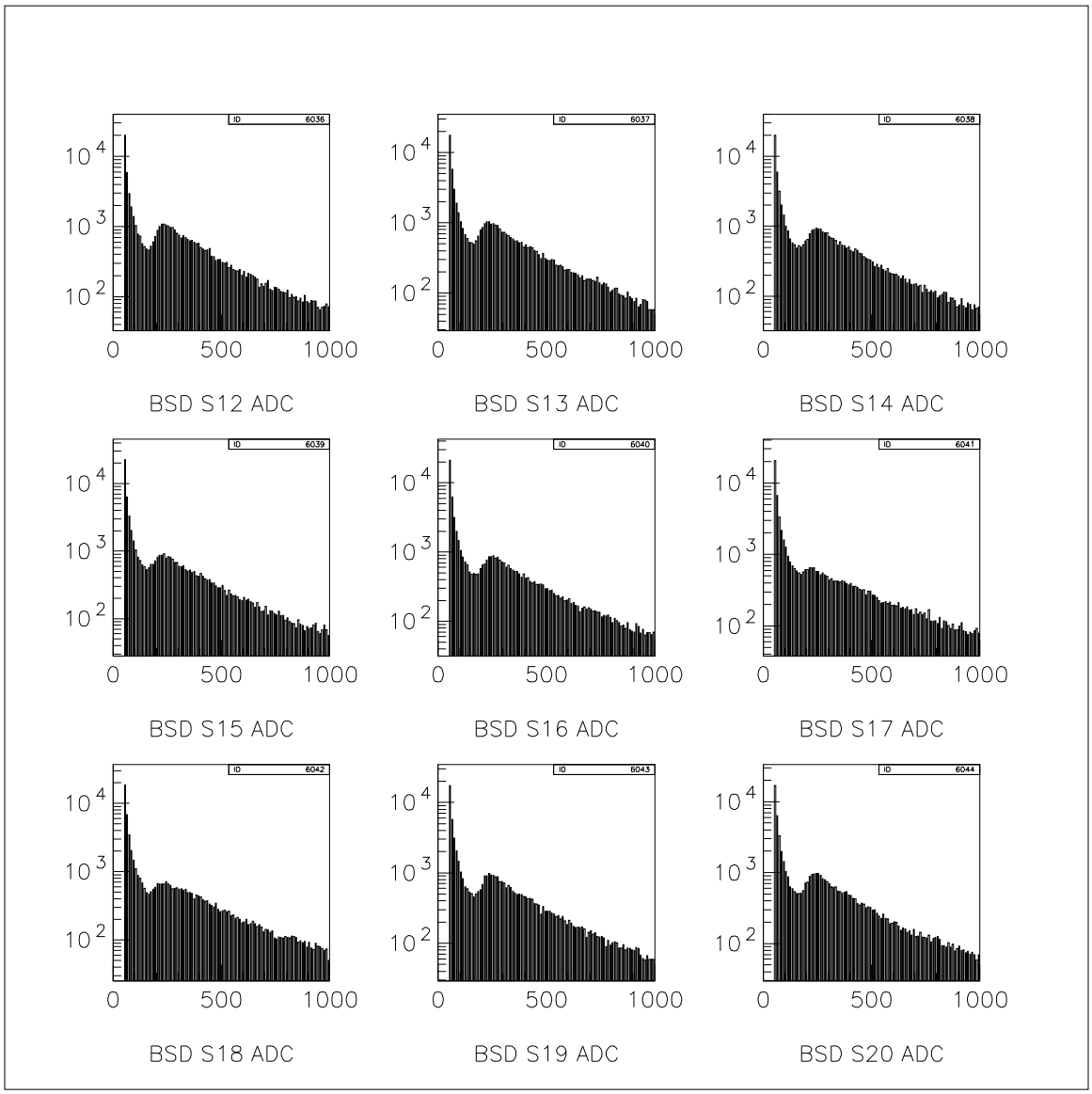
ID 6036
BSD S12 ADC
ID 6037
BSD S13 ADC
ID 6038
BSD S14 ADC
ID 6039
BSD S15 ADC
ID 6040
BSD S16 ADC
ID 6041
BSD S17 ADC
ID 6042
BSD S18 ADC
ID 6043
BSD S19 ADC
ID 6044
BSD S20 ADC
0
500
1000

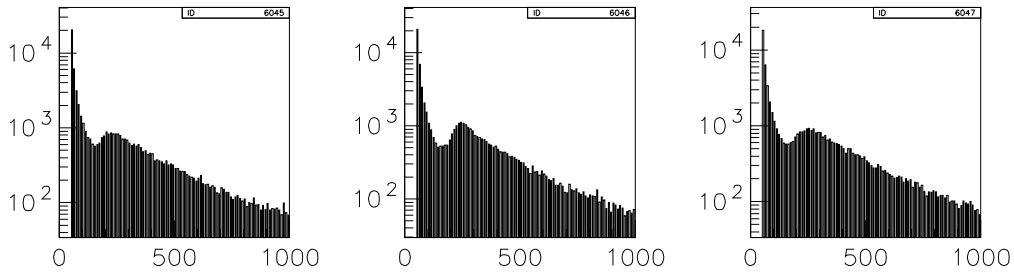

BSD S21 ADC BSD S22 ADC BSD S23 ADC

Bibliography

[1] H. Crannell, *et* al. CEBAF Proposal E-94-016 proposal to PAC-8 (1994). (unpublished).

[2] F. Close, N. Isgur and S. Kumano, Nucl. Phys. **B389**, 513 (1993).

[3] Perkins, Donald H. Introduction to High Energy Physics. 3rd ed. Menlo Park: Addison-Wesley, 1987.

[4] J. Napolitano and S. Godfrey, Rev. Mod. Phys. **71**, 1411 (1999).

[5] G. Janssen, B.C. Pearce, K. Holinde, and J. Speth, Phys. Rev. **D52**, 2690 (1995).

[6] S. Spanier, Phys. Atom. Nucl. **59**, 1291 (1996).

[7] S. Teige *et al.*, Phys. Rev. **D59**, 012001 (1999).

[8] Nathan Isgur, Kim Maltman, John Weinstein and Ted Barnes, Phys. Rev. Lett. **64**, 161 (1990).

[9] M.N. Achasov, Phys. Lett. **B440**, 442 (1998).

[10] C. Caso *et al.*, Eur. Phys. J. **C3**, 1 (1998).

[11] D.I. Sober *et al.*, Nucl. Instrum. and Methods **A440**, 263 (2000).

[12] Alex Dubanowitz, Senior project thesis, College of William and Mary, 1998. (unpublished).

[13] Johannes B. Ritter, Ph.D. thesis, University of Illinois at Urbana-Champagne, 1998. (unpublished).

[14] Richard Jones, David Hertzog, Johannes Ritter, Jetset Collaboration, 1998. (unpublished).

[15] D.W. Hertzog *et al.*, Nucl. Instrum. and Methods **A294**, 446 (1990).

[16] Robert A. Lindenbusch, Ph.D. thesis, Indiana University, 1996. (unpublished).

[17] Tom O'Connor, Senior project thesis, College of William and Mary, 1997. (unpublished).

[18] D.P. Heddle, Computers in Physics, **10**, 174 (1996).